Department of Precision and Microsystems Engineering

Towards prestressing neutrally stable joints with pressure

Kevin van Kesteren

Report no : 2025.055
Coach : Dr. Ir. G. Radaelli
Specialisation : Mechatronic System Design (MSD)
Type of report : Master Thesis
Date : 25-08-2025

Towards prestressing neutrally stable joints with pressure

Experimentation and parameter study on a spatial compliant enclosed volume joint

by

Kevin van Kesteren

Student number: 4580605
Thesis committee: Dr. Ir. G. Radaelli, TU Delft, chair, daily supervisor
Dr. J. Yang, TU Delft, external committee member
Specialisation: Mechatronic System Design (MSD)
Faculty: Faculty of Mechanical Engineering, Delft

Keywords: compliant mechanisms, neutral stability, close volume

TU Delft

Abstract

In the field of compliant mechanisms, neutrally stable mechanisms are gaining interest for among others increasing actuation efficiency, vibration isolation and their use in metamaterials. Prestressing these mechanisms is necessary to provide the potential energy they require to reach their state of neutral stability. Current prestressing methods are limited by their need for individual application or relatively long activation times and limited reversibility, limiting mechanisms which utilize a multitude of neutrally stable flexures. This research aims to design a neutrally stable, enclosed volume joint on which prestressing utilizing a negative internal pressure is tested. The joint is first characterized together with a parameter study, used to understand the influence of its geometry, and a finite element model, to assess its predictive accuracy. An experimental setup is constructed, which measures the torque-angle behavior of the joint under different prestress conditions. The results are compared to the expected behavior, which is closely resembled for some of the prototypes, while the simulations prove to be only indicative of the general trend.

Contents

1

Introduction

In the field of mechanical engineering, Compliant Mechanisms (CM) are increasingly researched and implemented as an alternative to traditional mechanisms. CM use the bending of flexible members, hereafter called flexures, instead of hinges and rigid bodies to achieve their motion. The advantages of using CM include a reduction in number of mechanism parts, increased compactness, low weight, low friction and a reduction in wear and backlash, which is desired in high-tech applications [1]. A challenge for CM can be their energy efficiency. A traditional mechanism providing a hinge function only has to overcome friction to be able to move, while the same CM essentially functions as a hinge and spring combined. To move the CM, bending has to occur which means strain energy is stored in the deformed mechanism. This energy can not always be recovered, which results in a higher energy demand compared to the traditional mechanism. To address the challenges of energy efficiency, a growing area of research within the CM field focuses on the development of neutrally stable mechanisms. Equivalent descriptions of neutral stability are continuous equilibrium, constant potential energy or a certain case of neutral stability, zero stiffness [2]. These mechanisms have constant potential energy over a certain range of motion if we assume they are isolated and conservative [3]. Constant potential energy means there are ideally no energy losses in the displacement range exhibiting this behavior. To reach the region of neutral stability from a relaxed state, potential energy first has to be introduced into the system, which can be done by prestressing the mechanism [4]. Bistable and by extension multistable mechanisms also require prestressing, but instead of a range of energetically equivalent positions, these are only stable at distinct points. Nevertheless, examples of these are described in addition to neutrally stable mechanisms, as they are commonly found in literature.

A prestress can be applied in the material, like the bistable composite tape-spring by Yang et al. [5]. In this case, heat treatment after initial fabrication introduces more internal stress, which can be tailored to result in self-deploying, neutrally stable and self-coiling structures. Important to note is that this process takes some time, in the order of hours, and can not be instantly reversed. Another way to induce residual stress in the material is exemplified by Kebadze et al. [6]. A similar tape-spring, fabricated from a homogeneous, isotropic shell is prestressed by applying deformations beyond its yield point. For the first bending moment this is done by again a heat treatment and for subsequent bending moments rollers are used. These can bend a single tape-spring, so scaling up the amount of strips to be prestressed would necessitate more rollers or prestressing one after another. A prestress can also be applied during assembly. Ammozandeh Nobaveh et al. [7] have made a compliant twisting beam which can be prestressed from positive to zero and negative stiffness by displacement on a threaded rod in the center axis of the beam. The prestress has to be applied manually by rotating a nut on the threaded rod, while an automated solution would look like a small actuator which turns the nut, which would have to be done for each nut individually, if prestressing multiple twisting beams. Another bi-stable twisting I-beam was made by Lachenal et al. [8]. The prestress was applied by fabricating initially cylindrical flanges, which were then assembled straight onto a web, forming the I-beam. The process of prestressing is not reversible and so is prone to stress relaxation, if continued use is envisioned. Another

way of applying mechanical prestress can be realized by using ”zero-length” springs, exemplified by Chaudhary et al. [9]. They made a neutrally stable unit cell by attaching zero-length springs to rigid elements. Assembling multiple of these unit cells will require increasingly more effort, so the method of prestressing does not scale well. Similarly, the curved compliant differential mechanism by Mak et al. [10] is prestressed using pretensioned springs. Chen et al. [11] made a variable stiffness joint, which can be tuned to behave neutrally stable, by sliding and consequently prestressing leaf springs. Again, these methods of prestress application are manual and individual per mechanism. Hamzehei et al. [12] have compiled design strategies for creating metamaterials with quasi zero-stiffness (QZS) behavior, which is a special case of neutral stability. QZS unit cells are designed to behave neutrally stable when loaded under tension or compression. The limit with these unit cells is that the behavior can not be turned off once implemented.

Looking at these examples and their limitations with regards to prestressing, a problem starts to emerge. An increase in the amount of neutrally stable flexures used in mechanisms could be highly beneficial to a variety of applications. Metamaterials could benefit from neutrally stable elements to achieve a wider range of tailored properties. High-precision stages benefit from actuation efficiency and vibration isolation, both of which neutrally stable mechanisms can provide. Mechanisms which try to limit actuation forces over certain displacement ranges, like exoskeletons also benefit. The limits of the above mentioned prestressing methods are that they often have to be done per individual mechanism, which means a scale-up in time or prestress tools when scaling up the amount of neutrally stable flexures. Further, the prestress method often has to be applied directly to the flexure by making contact, which limits the design flexibility, as the flexures have to remain accessible. The need for accessibility is of particular hindrance to metamaterials. A metamaterial is comprised of several unit cells which form a lattice structure [13]. By designing the unit cell to desired specifications, the resulting material can exhibit characteristics not found in conventional materials. If unit cells inside the lattice have to be accessed to be prestressed, there is a scaling problem. The number of unit cells the lattice is comprised of can only be so much as to allow the center unit cell to still be accessible. If there was a method of prestressing these flexures remotely, accessibility would not be a factor anymore and one could even envision flexures which are able to be turned on and off at command, behaving as a CM when turned off and additionally as a neutrally stable CM when turned on. In cases where this prestress can be applied remotely and to multiple flexures at the same time, the problem remains that this prestress is not easily reversible and takes some time, often in the order of hours.

In summary, there is a lack of methods for prestressing neutrally stable mechanisms which can target multiple flexures at once, remotely, reversibly and in a relatively small timeframe. To find a method which would be able to achieve this, a broad range of external stimuli can be considered. An external stimulus could enable the scaling up of the amount of neutrally stable flexures used in a given design and the simultaneous activation of these flexures. An external stimulus can be applied automatically and remotely, which enables more intricate designs. Examples of external stimuli include thermal stimuli, for which a few examples have been presented. These are relatively easy to apply, have short response times, but often require relatively large temperature differences, which might affect other properties and are not easily reversed. Another group is that of electrical stimuli, which are fast but have the disadvantage of small deformation ranges, which limits design scalability. They also need to have wiring added to where the current needs to be supplied. A light or chemically induced stimulus is often used in soft robotics, but the materials used here often suffer from long activation times and relatively low stiffness in all directions. This is undesirable as neutrally stable mechanisms only need to reduce stiffness in the desired direction while keeping the other stiffnesses high. Approaching the problem in terms of a pressure stimulus seems promising. The advantages of using pressure for prestressing include a large range of design dimensions, applicability for most materials and much better reachability of flexures compared to other methods.

In literature, advancements towards this idea can be found. Overvelde et al. [14] designed a transformable metamaterial which is actuated using inflatable air pockets on the hinges inside the unit cells. Pressurizing these causes the unit cell to flatten, transforming the shape and properties of the metamaterial at large. Sonneveld et al. [15] have made steps to design compliant rotational joints comprised of

closed fluid cells. These have a constant internal volume and utilize closed form pressure balancing to decouple stiffness and rotation. One could envision manipulating the internal volume and pressure, in addition to the design of the outer layer, to obtain a prestressed cell which might behave neutrally stable. Faltus et al. [16]have developed an analytical model for stiffness control in pneumatic metamaterials. By applying a varied pressure actuation, stiffness and behavior of the material could be chosen within the design limits. Designing a metamaterial which behaves neutrally stable with a certain pressure configuration could be possible with this.

From these examples, it seems working towards a mechanism in the form of an enclosed volume, for which internal pressure can be manipulated, could be a viable option to tackle the problem. If we base our flexure on a spatial joint with an enclosed volume, we can assume the joint behaves as a CM when the volume is equal to its starting volume, so the joint is unstressed. When the internal volume is now reduced in the closed joint, a negative pressure will start to affect it. This will apply a distributed load to the surfaces of the joint, causing deformation and thereby storing potential energy in the system, essentially prestressing it. If we assume that this joint has a region of neutral stability when prestressed, the negative pressure prestress will be able to deform the joint so it operates inside the region of neutral stability, requiring minimal actuation force to move. To test these assumptions, we want to measure the load-deflection curve of a spatial joint with an enclosed volume and a region of neutral stability when prestressed. This first has to be done from a relaxed state, so the initial behavior can be captured, and then from a state with the negative pressure prestress applied, so the influence of the prestress can be examined. This leads to the research goal.

1.1. Research goal

We want to test if the reduction of internal volume and resulting negative pressure on an enclosed volume joint, which has a region of neutral stability when prestressed, can be used as a means of prestressing it to operate inside the region of neutral stability. The research goal of this paper is to:

Design an enclosed volume joint which has a region of neutral stability when prestressed.

and

Test if a negative internal pressure can be used as a means of prestressing this joint so it behaves neutrally stable.

The approach is as follows: The load-deflection curve of spatial enclosed volume joint prototypes is experimentally characterized under varying design parameters and prestress levels to evaluate the influence of internal volume and geometry on joint mechanics. Results are compared with a finite element model to assess its predictive accuracy for parameter variations.

1.2. Paper outline

In chapter 2, the enclosed volume joint is introduced with its relevant parameters, followed by a parameter study to understand the influence of certain parameters on the load-deflection behavior of the joint. Here, also the experimental setup, -protocols and finite element analysis are detailed. The results of the experiments and simulations will be given in chapter 3. In chapter 4, comparisons will be made between different results and simulations and their implications and accuracy discussed. Lastly, in chapter 5, the paper will be concluded.

2

Methods

An experimental setup is established using an enclosed volume joint, to measure the load-deflection curve under various prestress conditions. In this chapter, the enclosed volume joint will first be introduced and its parameters defined in section 2.1. Secondly, to understand the influence of certain parameters of the joint with respect to the load-deflection characteristic, a parameter study will be detailed in section 2.2. Thirdly, the fabrication of prototype variants and the experimental setup is explained in section 2.3. Lastly, a finite element analysis, which might predict the effect of other parameter variations is introduced in section 2.4.

2.1. Enclosed volume joint

The geometry presented in Figure 2.1 forms the basis of the enclosed volume joint explored in this research. Its base shape is a cube with pyramid-shaped indents on 4 of its 6 sides. In Figure 2.1a, the previously discussed shape is visualized, opposite sides of the joint match color, the top plate is transparent in this figure. The triangles that form the pyramid-shaped indents, are hold together by creases between the triangles. The geometry is thus hollow, which results in an enclosed volume, visible in Figure 2.1b. At all creases between the plates, a low stiffness connection is assumed, which means they deform relatively more. Upon prescription of a positive or negative rotation around the z-axis on the, here transparent, top plate, the joint will rotate and consequently translate in negative z-direction.

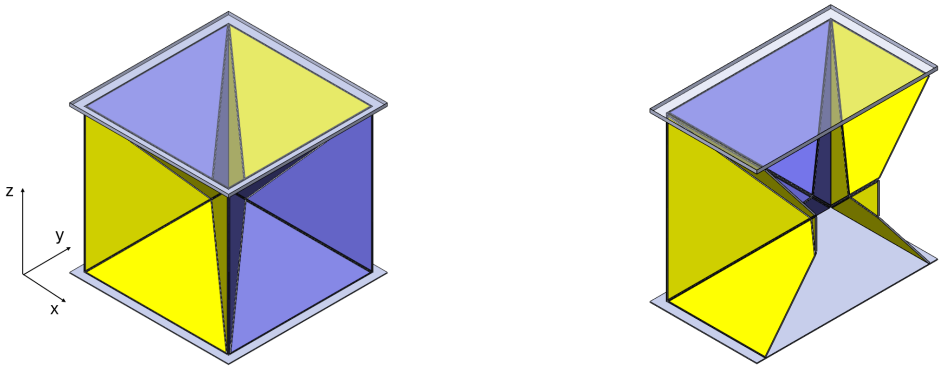

(a) Isometric view.

(b) Cross-section isometric view.

Figure 2.1: Different views of the geometry of the enclosed volume joint.

As the rotation of this joint has the largest range of motion, the torque-angle behavior is examined in this case as its load-deflection curve. In preliminary prototyping it was observed that the joint exhibited a torque-angle behavior like the one visualized in Figure 2.2.

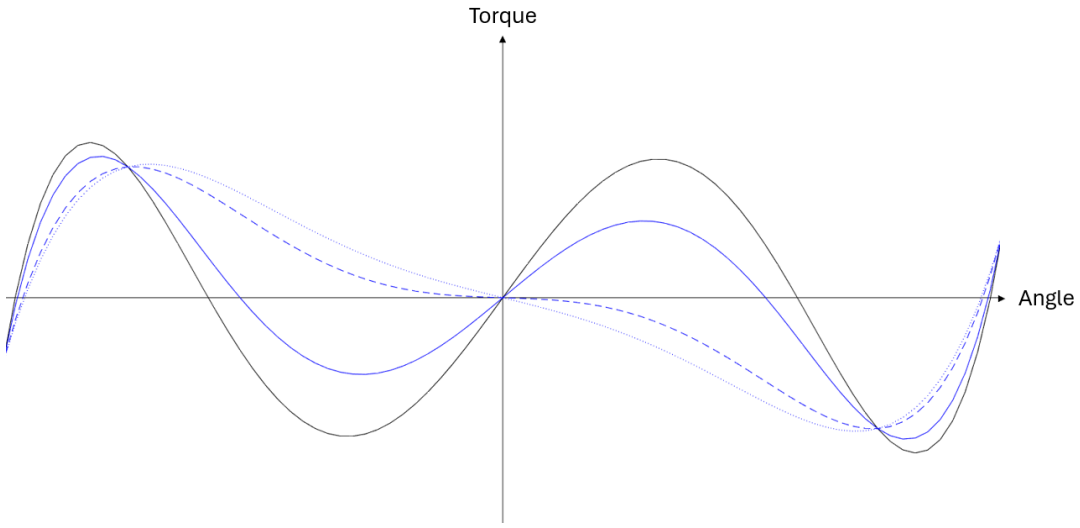

Figure 2.2: Expected torque-angle curve of the enclosed volume joint. The black curve represents the behavior of the unstressed joint. The sequence of the solid, dashed and dotted blue curves indicate the expected change that will occur with increasing prestress.

The behavior is characterized by 5 equilibrium points, with the first point at the origin being its starting position. As the behavior is mirrored around the origin, it is explained in the direction of positive angle. Upon gradual rotation to a positive angle, the required torque initially increases until a maximum, after which it decreases to the following equilibrium point. The point occurs at around halfway the maximum possible rotation and represents the moment the positive actuation torque changes into a negative torque, the actuator is ”pulled” by the joint. An decrease in actuation torque is observed until a minimum, after which it increases again until it reaches the last equilibrium point. From this point the torque increases exponentially, as it represents the moment the indents of the joint touch each other and are no longer free to move. It is expected that the introduction of a prestress on the joint will lead to the behavior indicated by the sequence of solid, dashed and dotted blue curve. The slope around the origin is reduced to a possible neutrally stable position and upon further prestressing might even flip into the opposite direction, creating a bistable joint. The rotating motion of the joint can be seen in Figure 2.3.

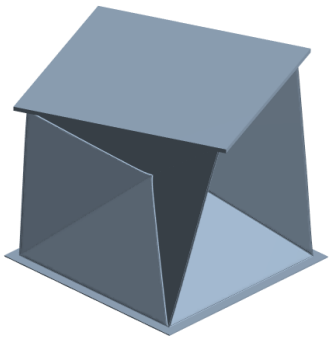

Figure 2.3: Top-angled view of the rotating motion of the enclosed volume joint.

As previously mentioned, the pyramid-shaped indents are comprised of triangles, held together by creases. In Figure 2.4 one of these triangles is depicted with relevant parameters. The base of the triangle has length L, which results in a cube of dimensions L x L. The angle α of both corners at the triangle base and thickness t of the triangles are the parameters explored in the following experiments. The angle α is related to the angle of indentation and will determine how deep the indents will be, resulting in more or less internal volume. The thickness t of the triangles will determine how stiff the triangles are compared to the creases.

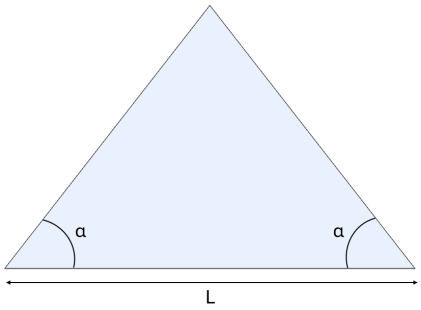

Figure 2.4: Single triangle which makes up the indented sides of the enclosed volume joint with parameters.

To calculate the resulting internal volume of the joint we subtract the external volume of the indented sides from the volume of an unindented cube in

$$V_{\text{int}} = V_{\text{tot}} - V_{\text{ext}} \tag{2.1}$$

,for which we can write out the terms

$$V_{\text{int}} = L^3 - \frac{4}{3}L^2\sqrt{(\frac{1}{2}L\tan(\alpha))^2 - (\frac{L}{2})^2} \tag{2.2}$$

which result in

$$V_{\text{int}} = L^3(1 - \frac{2}{3}\sqrt{\tan^2(\alpha) - 1}) \tag{2.3}$$

2.2. Parameter study

To test if a neutrally stable enclosed volume joint can be prestressed using a negative internal pressure, the required torque during rotation is measured. This is done without prestress and with prestress of different magnitudes. The trend in required actuation torque compared to the magnitude of prestress gives an indication of the validity of the expected curve. The parameter study is conducted to study the influence of different parameter values on the torque-angle characteristic and the region of neutral stability. For this study length L is kept constant at L = 100 mm. The variables that are changed are α, which in turn changes the internal volume V_{int}, and the thickness t of the plates. The internal volume is presented as a fraction

$$f = \frac{V_{\text{int}}}{V_{\text{max}} - V_{\text{min}}} \tag{2.4}$$

between the minimum possible internal volume ($V_{\text{min}} = \frac{1}{3}$ l) and the maximum internal volume ($V_{\text{max}} = 1$ l), both visualized in Figure 2.5.

Table 2.1 shows the different variations, indicated by the abbreviation Var 1, 2, etc., of the enclosed volume joint with parameters and their values.

Table 2.1: Variations of the enclosed volume joint prototypes with corresponding parameters

		Internal volume fraction (f)		
		0.201 (α=52°)	0.238 (α=51.5°)	0.276 (α=51°)
Thickness (t)	0,5mm	Var 1,2,3	Var 5	Var 6
	0,8mm	Var 4		

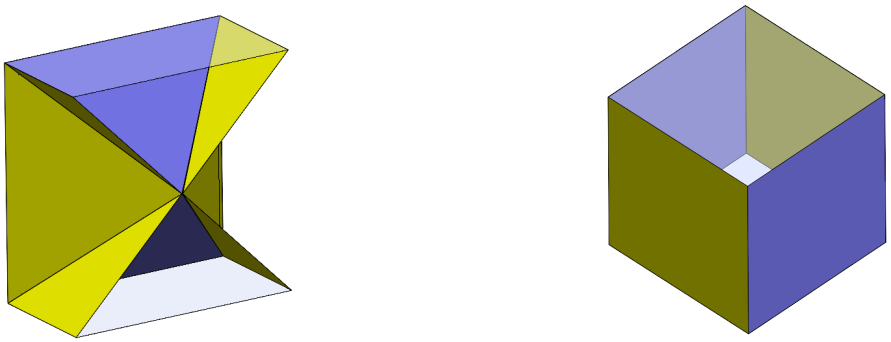

(a) (b)

Figure 2.5: (a) Cross-section of the enclosed volume joint with the minimum possible internal volume V_{min} and (b) top-angled view of the joint with the maximum possible internal volume V_{max}.

2.3. Fabrication and experimental setup

2.3.1. Prototype fabrication

The prototypes are made out of flat PP plates. The PP plates are cut into the desired dimensions and joined together by strips of duct tape to form the enclosed volume joint, see Figure 2.6. This process is carried out with PP plates with thickness $t = 0.5$ mm and $t = 0.8$ mm, as follows from Table 2.1.

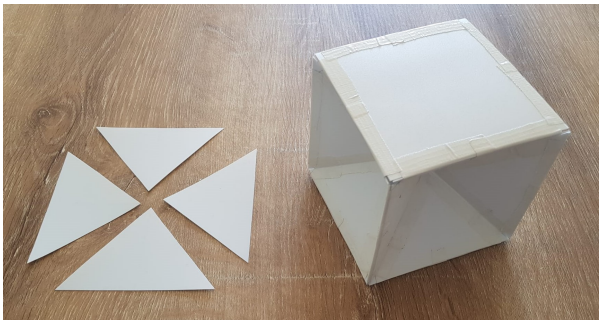

Figure 2.6: Side panels and complete prototype of enclosed volume joint.

2.3.2. Experimental setup

To be able to prestress the joint, the volume inside needs to be extracted. Therefor an enclosed volume had to be constructed around the prototypes, as the joint itself is not airtight. This is done by first fabricating a top and bottom plate, made of PMMA of 3 mm thickness. These plates are attached to the flat sides of the joint with duct tape. Then, a flexible polyethylene sheet is cut to the desired dimensions and joined to the top and bottom to the PMMA plates using double-sided tape based on acrylic adhesive with a synthetic rubber body. The seams and corners are then sealed using a liquid rubber sealant which hardens upon drying. A close-up of the sealed polyethylene sheet can be seen on the left side of Figure 2.7a. A valve is pressed through the polyethylene sheet and fastened to be able to connect a tube. The prototype is then left to dry for the rubber sealant to harden. When the sealant is sufficiently hardened, the prototype is checked for leaks by submersion in water. The enclosed volume is put under positive pressure, so escaping air can point to the location of potential leaks. A complete prototype of the enclosed volume joint can be seen on the right side of Figure 2.7a.

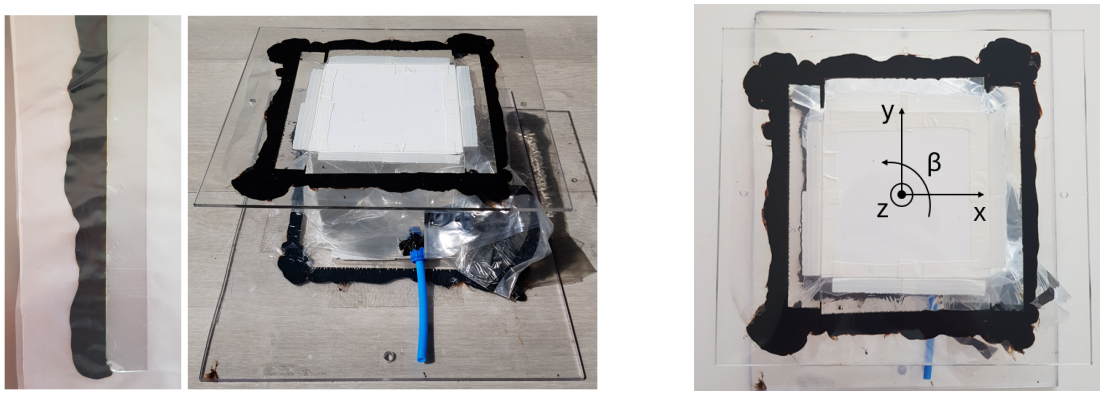

(a) (b)

Figure 2.7: (a) (Left) Close up of polyethylene sheet sealed by double-sided tape and rubber sealant. (Right) Prototype with seals and air tube visible. (b) Coordinate system and starting position of the joint during testing.

With the prototype able to be prestressed, the rest of the experimental setup has to be constructed to measure the torque at different angles. The torque sensor used in this research is an HBM T20WN torque transducer with a nominal torque of 0.5 Nm. In practice this translates to a torque limit of $\pm$450 Nmm. To interface the sensor with the prototype, it is clamped to a beam which is fastened to the bottom PMMA plate. The input rotation is applied at the top of the prototype via a custom-designed connector. This component has two requirements: (1) permit vertical translation of the top plate in the z-direction during joint rotation (as shown in Figure 2.7b), and (2) minimize friction, as it also serves as the rotational force arm. To meet these requirements, the piece in Figure 2.8 was designed. One end clamps to the rotation actuator, while the other houses smooth rods inserted into predrilled holes, as seen in Figure 2.8b.

(a) (b)

Figure 2.8: (a) Coupling piece in its separate parts and (b) as a whole.

At the top PMMA plate, vertical rods are fastened which are able to slide along the parallel rods of the connector during translation of the prototype in z-direction. Lastly, to extract air and consequently prestress the joint a syringe is connected to the valve, which allows for relatively more accurate prestressing compared to a pump. The complete test setup can be seen in Figure 2.9.

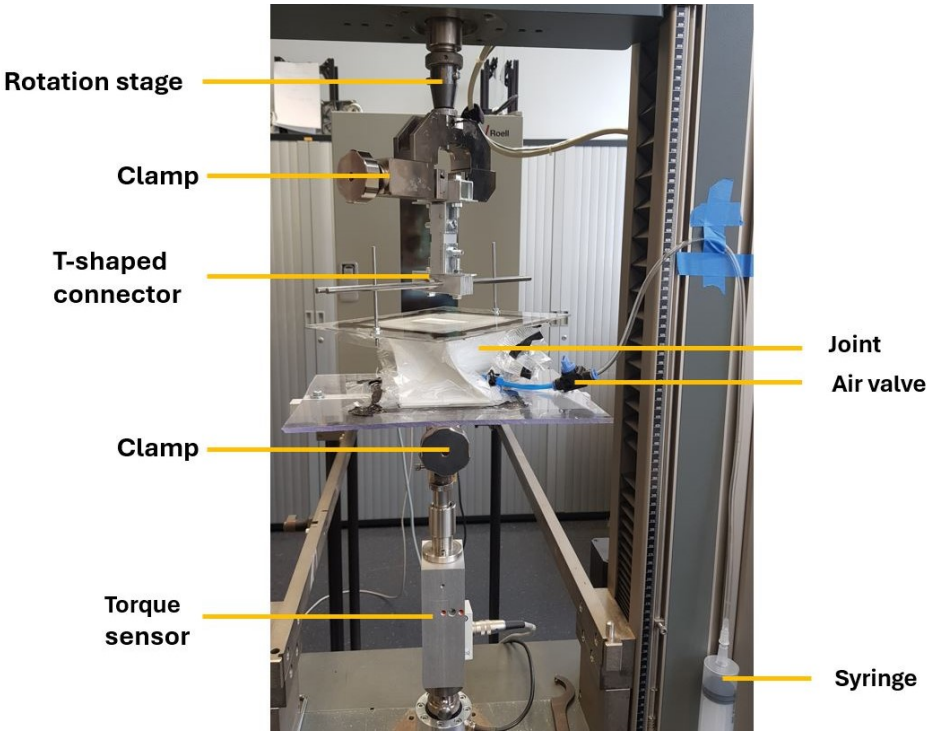

Figure 2.9: Complete test setup of the enclosed volume joint.

2.3.3. Experiment protocols

To study the relation of prestress and required actuation torque, the prototype variants are tested unstressed with an open volume and with different magnitudes of prestress and a closed volume. The joint is rotated and its torque-angle curve measured. Rotation occurs around the z-axis, indicated by β, as illustrated in Figure 2.7b. The different increments of β are given in Table 2.2. The process of prestressing is conducted as follows: The torque sensor is first calibrated to measure 0 $\pm$2 Nmm torque in the starting position β_0 with the valve opened. Then, a rotation to β_{pre}, which is increased each experiment, is imposed. After this, a pause is programmed in, during which air is extracted using a syringe until the polyethylene sheet wraps around the deformed volume and a steady-state torque value of about 0 Nmm is reached again. The valve is closed from here on to preserve the prestressed state.

Table 2.2: Experiment protocols followed for each prototype.

		β_0	β_{pre}		β_0	β_1	β_2	β_3	β_4	β_0
Experiment 1	valve open	n.a.	n.a.	air extracted valve closed	0	45	-45	45	-45	0
Experiment 2		0	10		0	45	-45	45	-45	0
Experiment 3		0	20		0	45	-45	45	-45	0
Experiment 4		0	30		0	45	-45	45	-45	0
Experiment 5		0	40		0	45	-45	45	-45	0

Following the pause a rotation back to the starting position β_0 is imposed. From this starting position, two complete measurements are conducted, which means a rotation to β_1, followed by a rotation to the other end β_2, and subsequently β_3 and β_4. From here, a rotation back to the starting position β_0 is imposed. For most of the prototypes, all the experiments are repeated two times.

2.4. Finite element analysis

To construct a finite element analysis which might predict other variations in parameters, a model of the geometry was made in SolidWorks. The geometry was modeled as a homogeneous solid and analyzed as such. The advantage of this is that connections between creases and plates, or only between plates in a simplified model, do not have to be defined, which simplifies the setup of the model. A close-up of some creases in the solid model can be seen in Figure 2.10a, as well as a close-up of the mesh in Figure 2.10b. The creases are significantly thinner than the plates, so fillets at the transitions have been added. This should results in a more stable solver, as sharp transitions can often cause problems. The implications of modelling the joint like this are discussed in chapter 4.

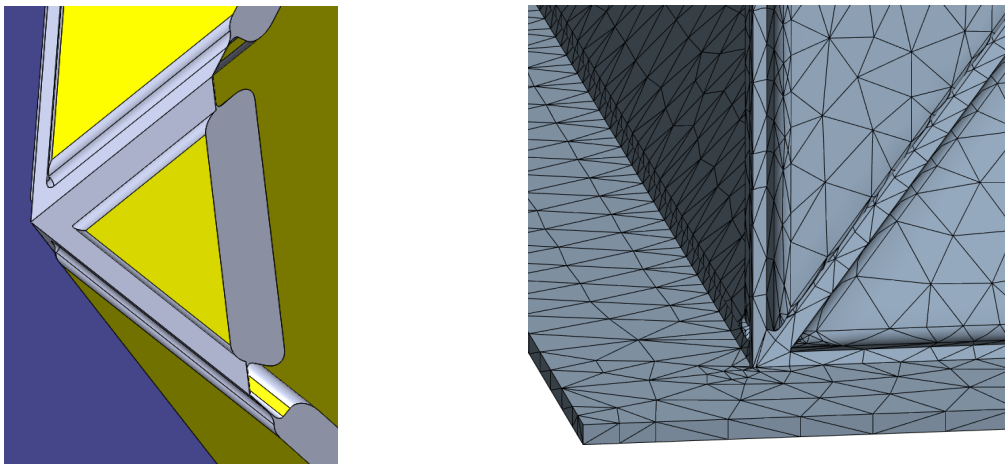

(a) (b)

Figure 2.10: (a) Close-up of some creases and (b) of the mesh at a corner of the joint.

The SolidWorks geometry is imported to ANSYS Mechanical and given the following material properties: a Young's Modulus of 1.46 GPa and Poisson's Ratio of 0.4087. This corresponds to a low flow, homopolymer PP in the ANSYS database. To constrain the geometry, the bottom plate is modeled as a fixed support, which means this plate is unable to translate, rotate or deform. At the top plate, a prescribed rotation is imposed, as seen in Figure 2.11a. The top plate is still free to move in every other direction and deform, but to compensate this freedom, it has had its thickness increased compared to the general thickness t. The prescribed rotation increases linearly from 0° to 40° in 400 timesteps, so 1° per 10 timesteps.

At the indented sides, as well as the top and bottom plate, a pressure normal to the plates is imposed, as seen in Figure 2.11b. The pressure stays 0 Pa for the first 10 timesteps and then increases linearly beginning at timestep 11. It increases by 100 Pa per timestep up to a value of 1000 Pa for the first prestress condition and 3000 Pa for the second prestress condition, which is a separate simulation. The specific pressure build-up means that for both cases pressure is not imposed until 1° of rotation has been completed, which is done to avoid unsolvable starting conditions, as in reality the joint will also not be perfectly symmetrical. Having a symmetrical joint with a pressure of equal directions and load can lead to a situation where multiple deformations are equally possible and the model not being able to decide between them.

After the pressure reaches the desired value, it is held constant at that value for the remainder of the test run. The direction of pressure is modeled to be normal to the deformed geometry, so its direction will change depending on the local deformation. To extract the torque-angle curve a moment reaction probe is defined on the top plate and on the fixed support boundary condition, to see if the reaction forces match.

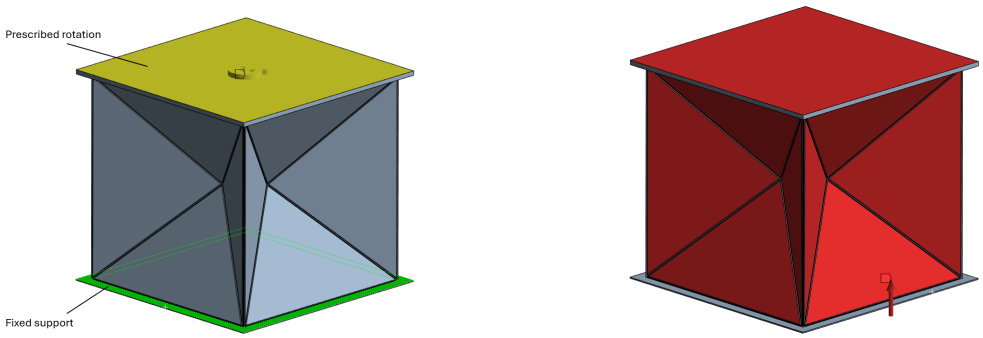

Figure 2.11: (a) Finite element model of the joint with a prescribed rotation on the top plate and a fixed support boundary condition on the bottom plate and (b) the normal pressure acting on all sides of the joint (the normal pressure on the bottom plate here indicated by the red arrow).

3

Results

This chapter presents the results of this study. Section 3.1 functions as a reading guide and describes the process of data selection for the experiments and simulations. Section 3.2 shows torque-angle graphs of all the tested prototypes, while section 3.3 shows comparisons between selected prototypes. Lastly, section 3.4 visualizes the results of the finite element model.

3.1. Data selection

To reduce data clutter and improve readability of the experiment results, several data processing steps are applied. First, the prestressing phase which involves rotating to a set angle, extracting air, and returning to the initial position, is excluded from the graphs. The raw data of the experiments is given in Appendix A. Second, averages of the data have been calculated which cancel out effects like hysteresis. Calculating the average starts by selecting the data from on cycle forth and back from data point β_2 up to β_4 as in Table 2.2. Effects at the start of the test are also neglected this way. A moving mean with a window of 10 datapoints is imposed upon the raw data and from this mean data an average curve is calculated.

The data for each prototype is presented in two graphs: The top graph visualizes the raw data, excluding the prestressing phase as described above, as well as the averages. One complete test per interval of prestress is given with its corresponding average. In the bottom graph, only the average curves are visible to get a clearer picture of the change in torque-angle behavior of the joint. The following naming convention has been followed in the legend: the value of thickness t in mm, internal volume fraction f and the degree of prestressing, indicated by $number$vac ($number$ being the angle in degrees used for prestressing). Test runs without a vac-indication are done without prestress. The descriptions under the graphs indicate which prototype variation is presented, named Var1, Var2, etc. Corresponding parameters for each variation can be found in Table 2.1 as well as in the descriptions.

3.1.1. Finite element model data

For the simulations, the following data is collected: First, a comparison of the base joint Var1 with crease thicknesses of 0.1 mm, 0.05 mm and 0.01 mm. This comparison is made to choose the crease thickness for the rest of the models, which is set at 0.05 mm. Second, a comparison between positive and negative pressure values on the base joint Var1, to confirm that the direction of pressure is chosen correctly in the model and reflects the expected trend. Third, a comparison between different internal volume fractions f, corresponding to variations Var1, Var5 and Var6. And lastly, a comparison between the different plate thicknesses t, corresponding to variations Var1 and Var4.

3.2. Prototype results

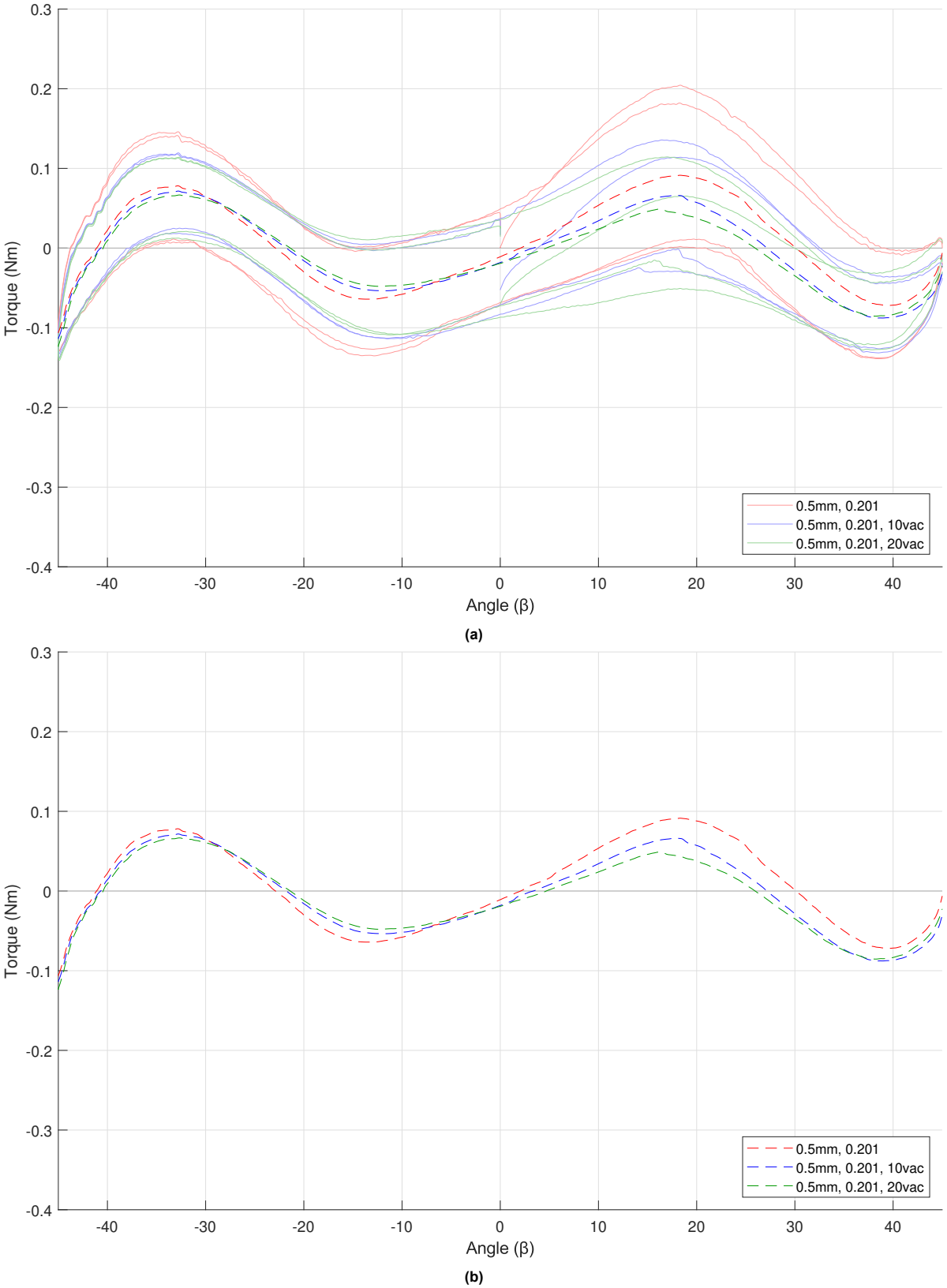

Figure 3.1: (a) Joint Var1 with parameters t: 0.5 mm, f: 0.201, visualized with all data and (b) with averages only.

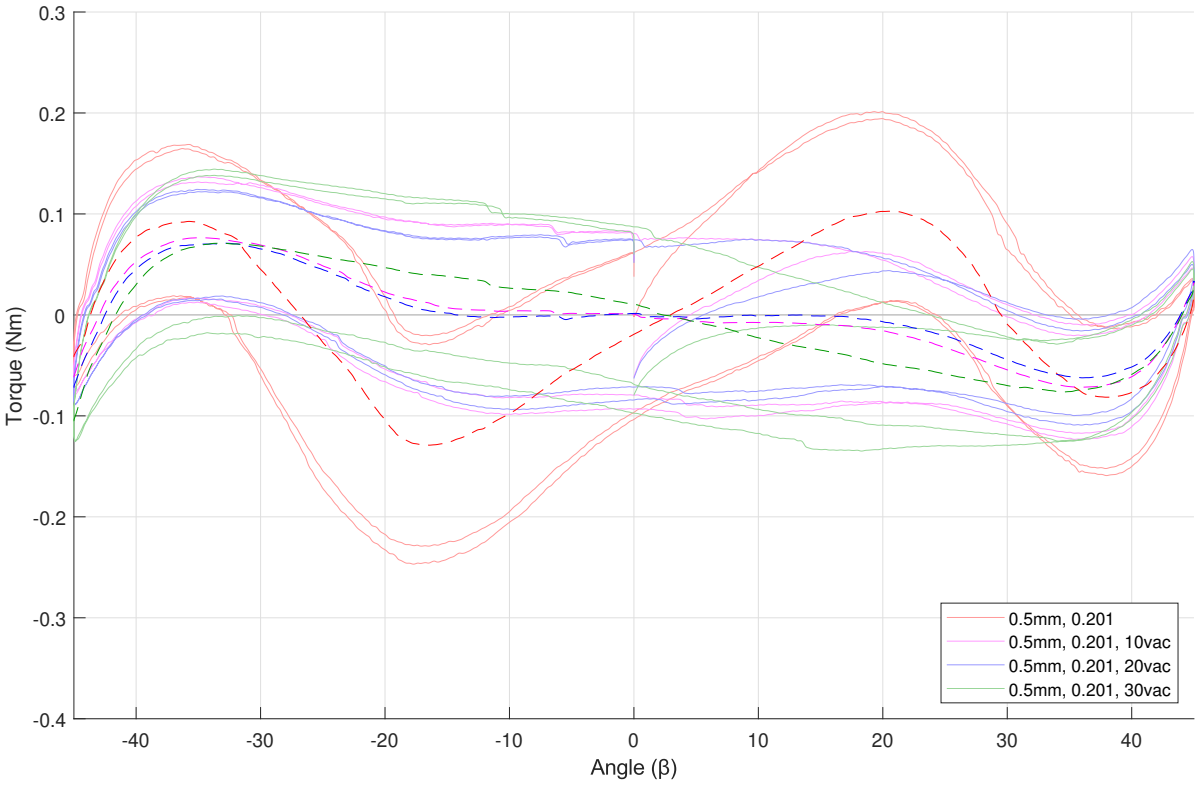

(a)

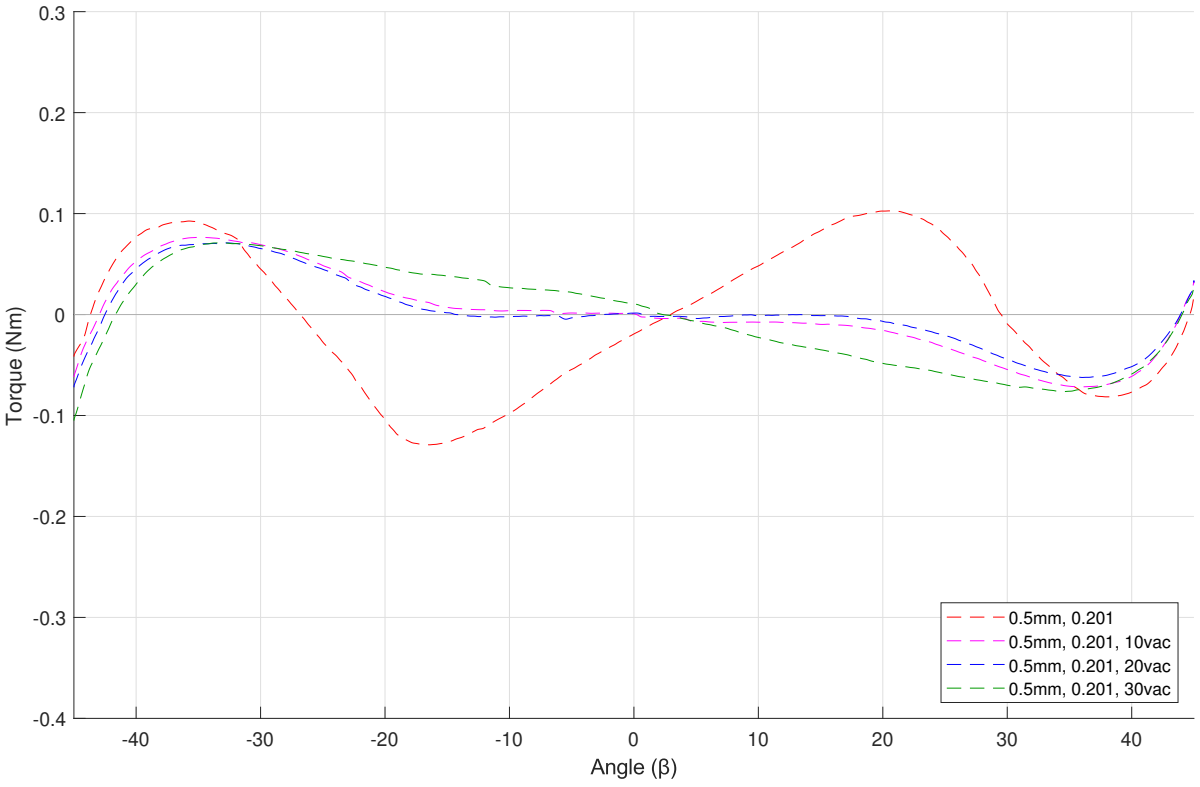

(b)

Figure 3.2: (a) Joint Var2 with parameters t: 0.5 mm, f: 0.201, visualized with all data and (b) with averages only.

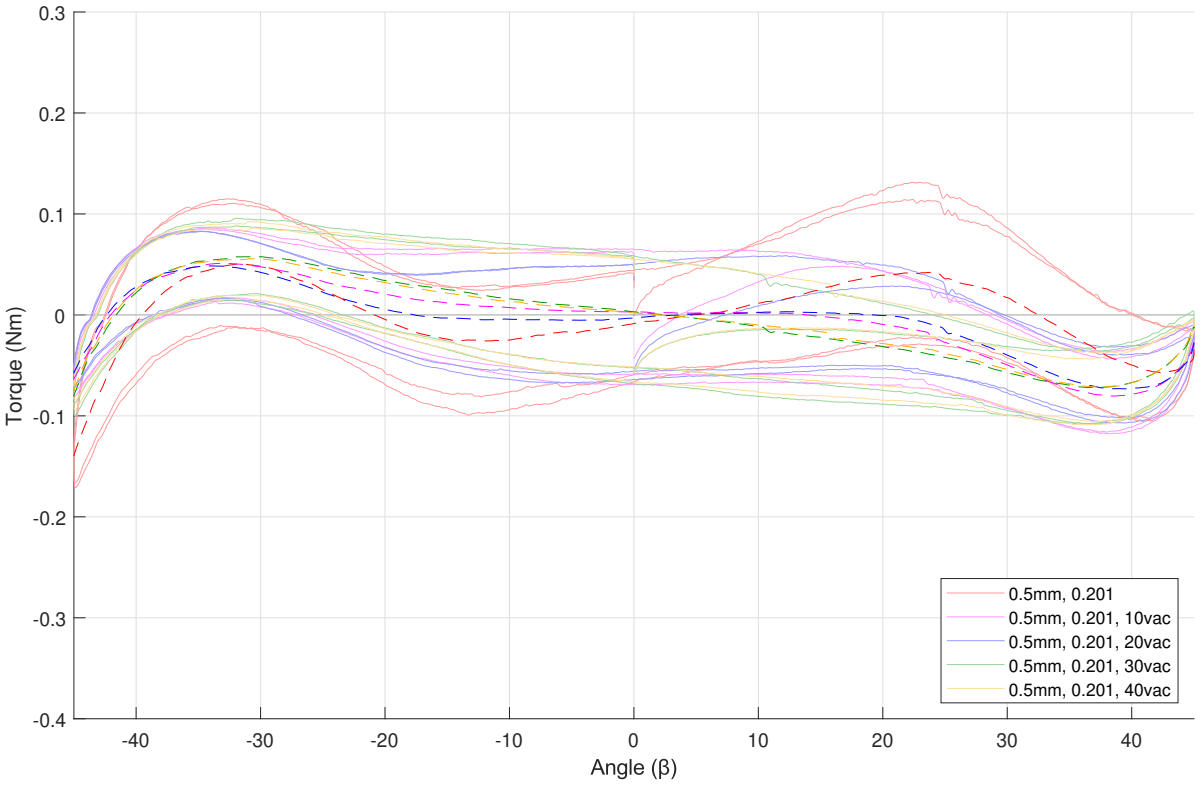

(a)

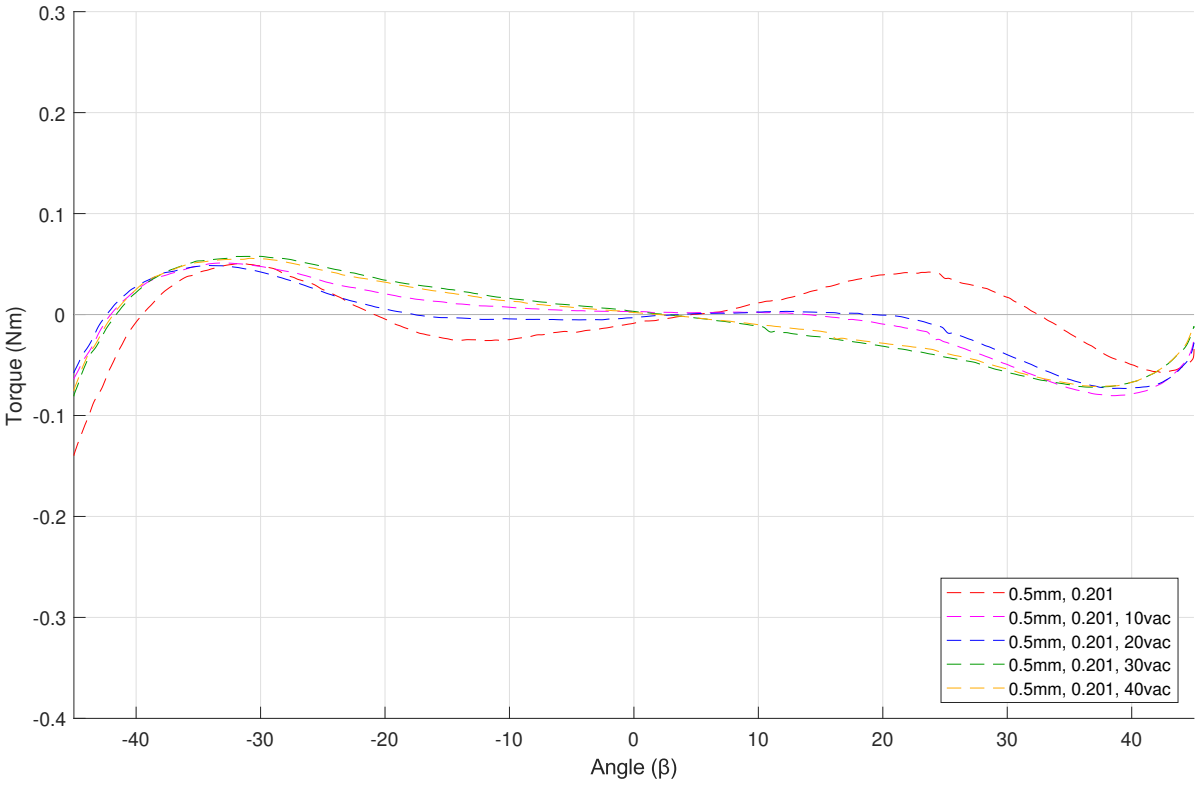

(b)

Figure 3.3: (a) Joint Var3 with parameters t: 0.5 mm, f: 0.201, visualized with all data and (b) with averages only.

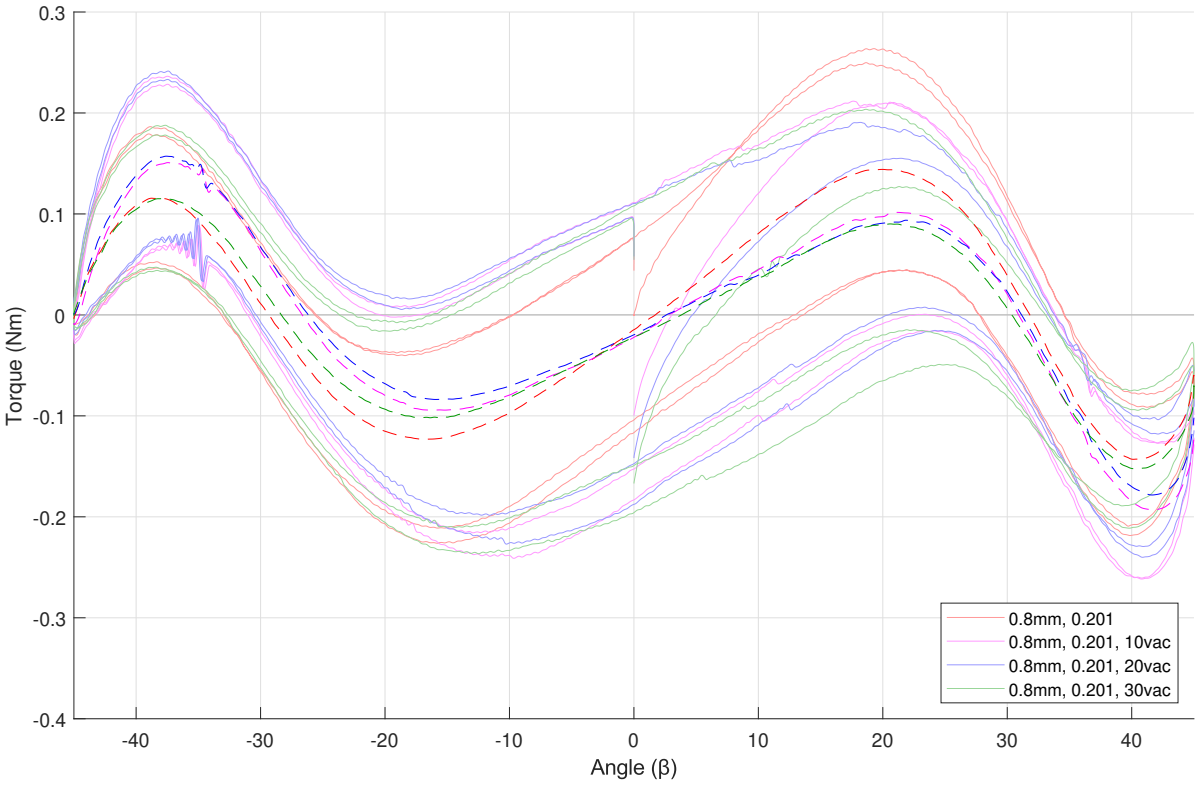

(a)

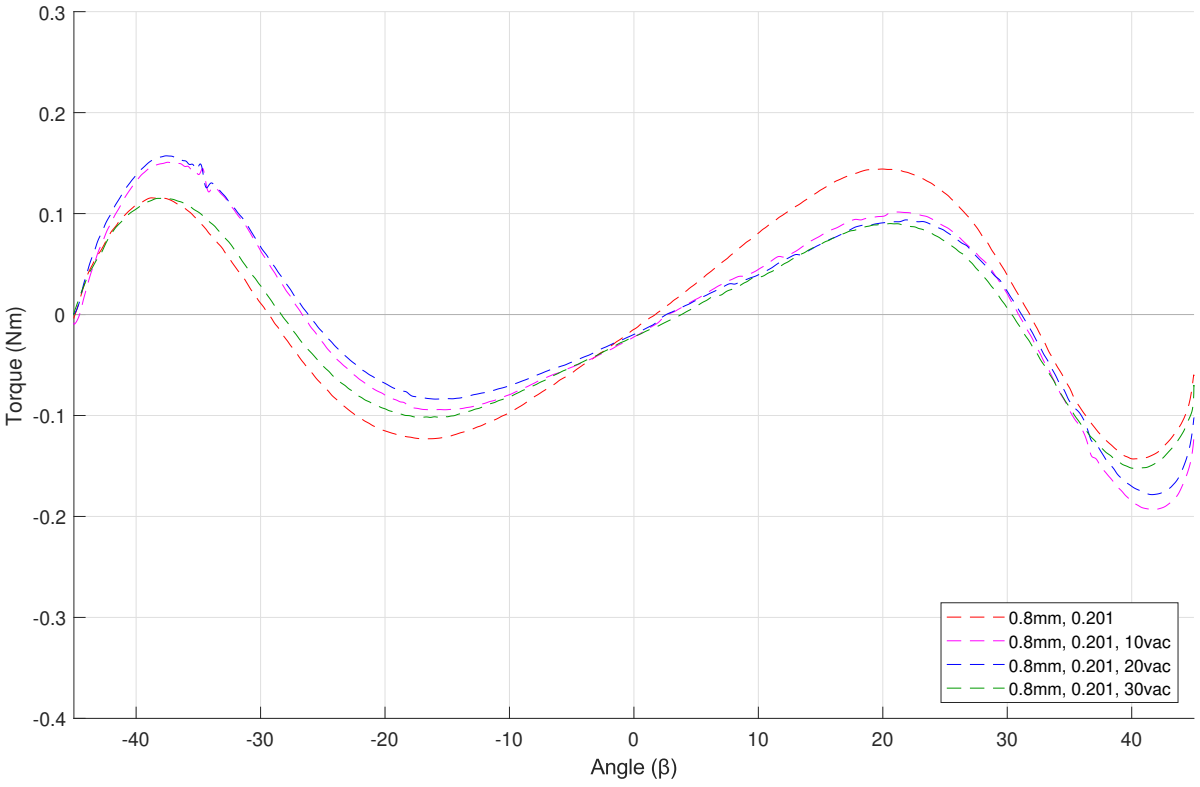

(b)

Figure 3.4: (a) Joint Var4 with parameters t: 0.8 mm, f: 0.201, visualized with all data and (b) with averages only.

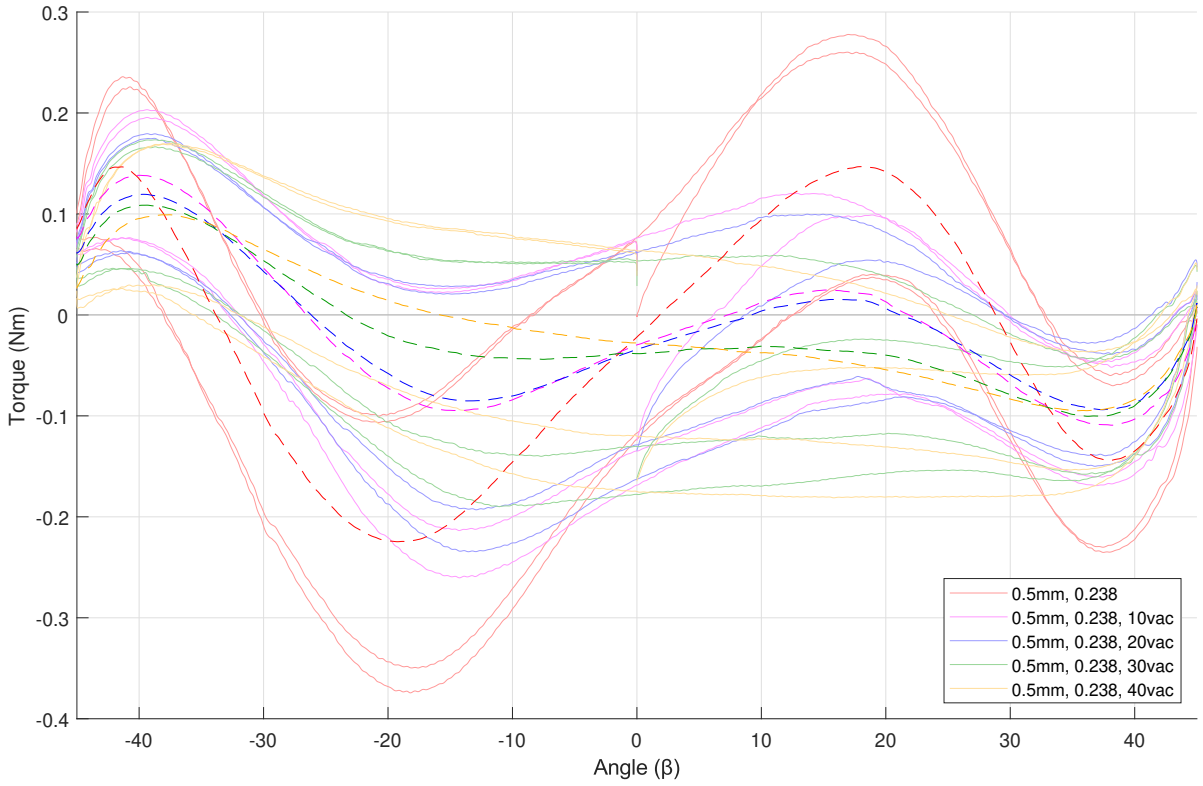

(a)

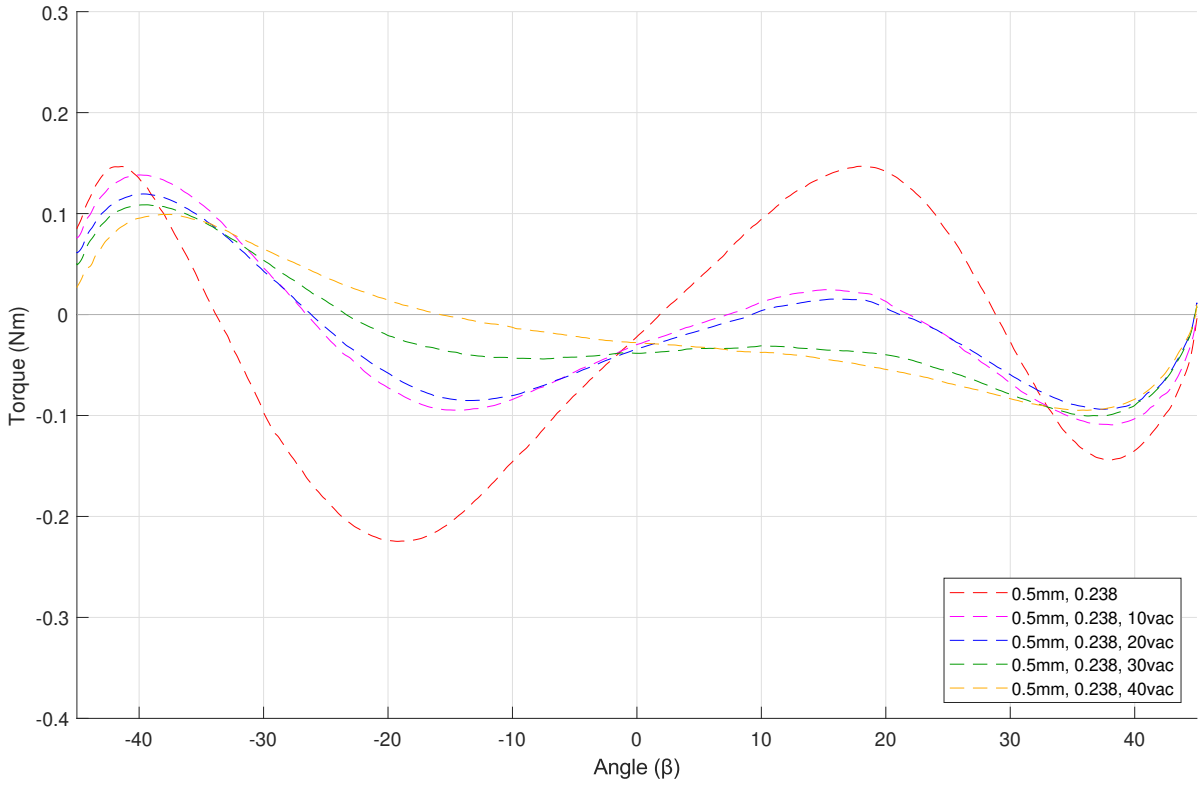

(b)

Figure 3.5: (a) Joint Var5 with parameters t: 0.5 mm, f: 0.238, visualized with all data and (b) with averages only.

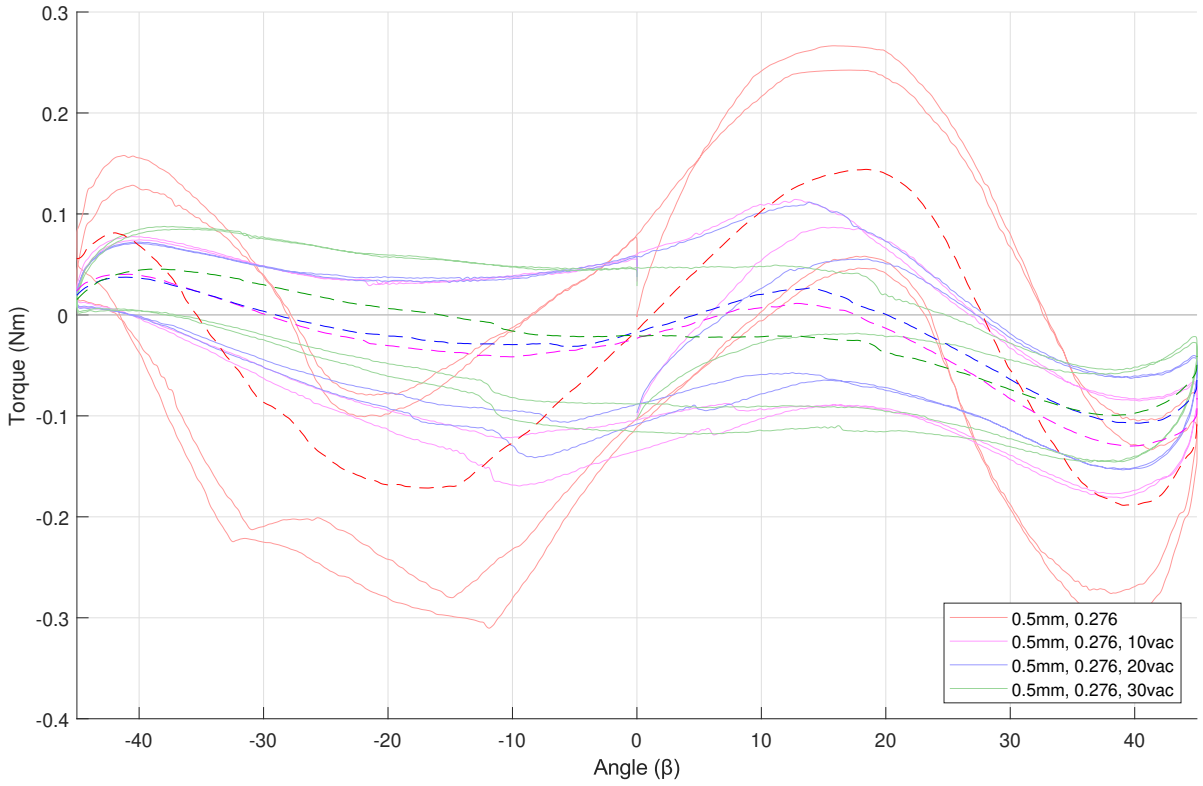

(a)

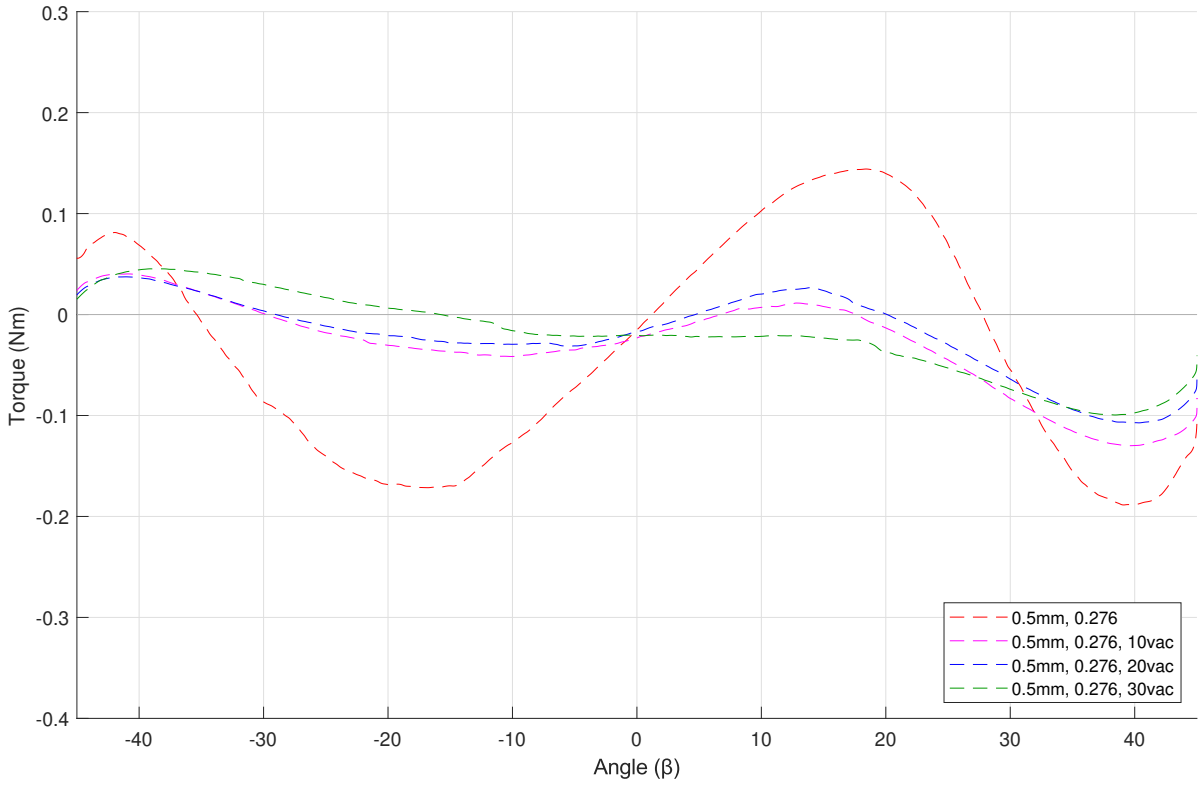

(b)

Figure 3.6: (a) Joint Var6 with parameters t: 0.5 mm, f: 0.276, visualized with all data and (b) with averages only.

3.3. Parameter comparison

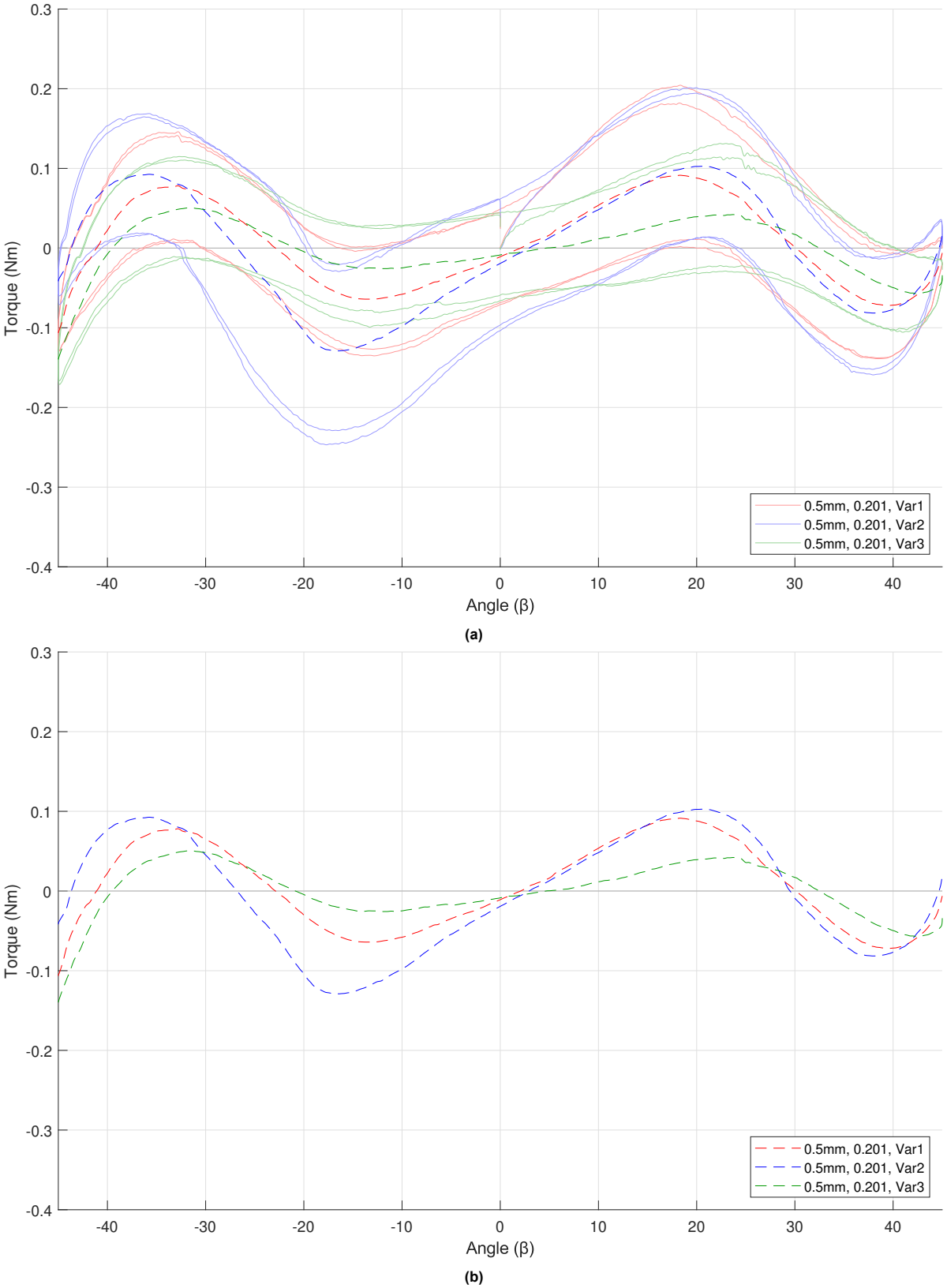

Figure 3.7: (a) Joints Var1, Var2 and Var3 with parameters t: 0.5 mm, f: 0.201, visualized with all data and (b) with averages only.

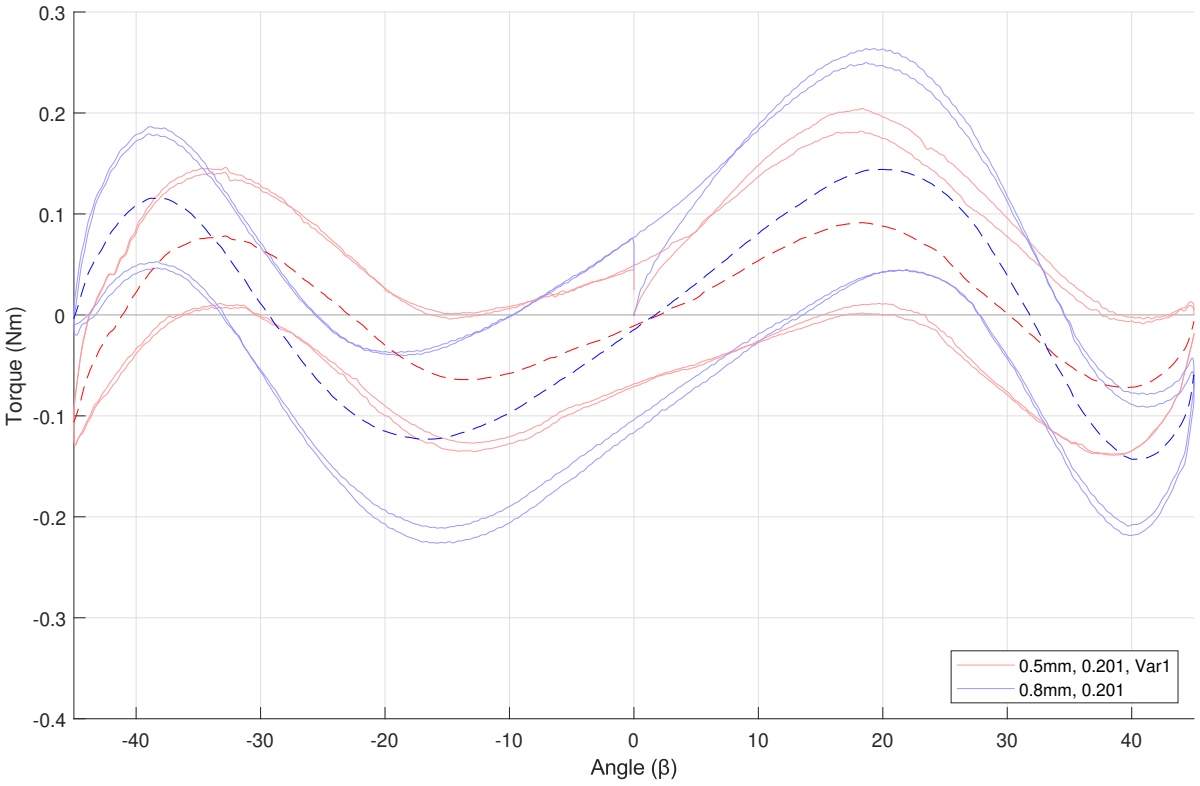

(a)

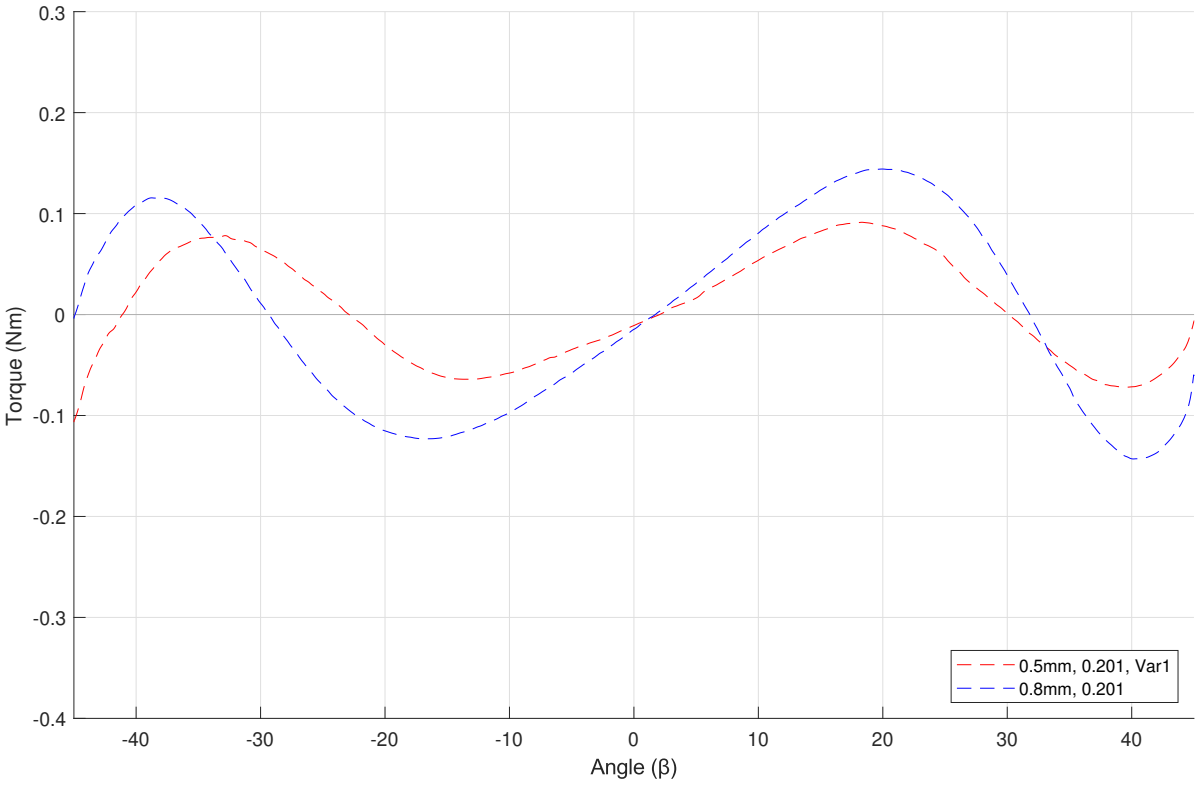

(b)

Figure 3.8: (a) Joints Var1 and Var4 with parameters t: 0.5 mm, t: 0.8 mm and both f: 0.201, visualized with all data and (b) with averages only.

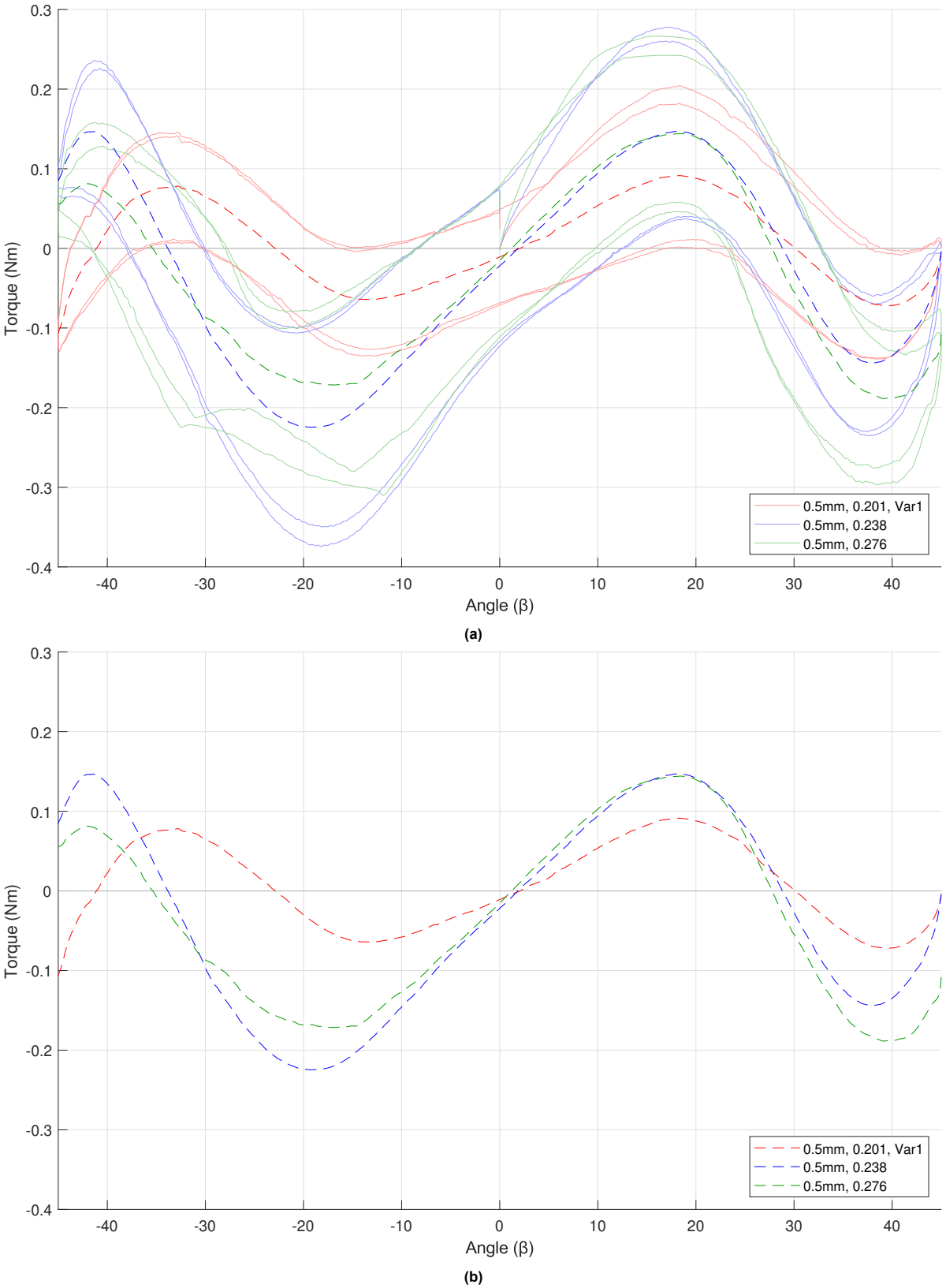

Figure 3.9: (a) Joints Var1, Var5 and Var6 with parameters t: 0.5 mm, f: 0.201, f: 0.238 and f: 0.276, visualized with all data and (b) with averages only.

3.4. Finite element analysis results

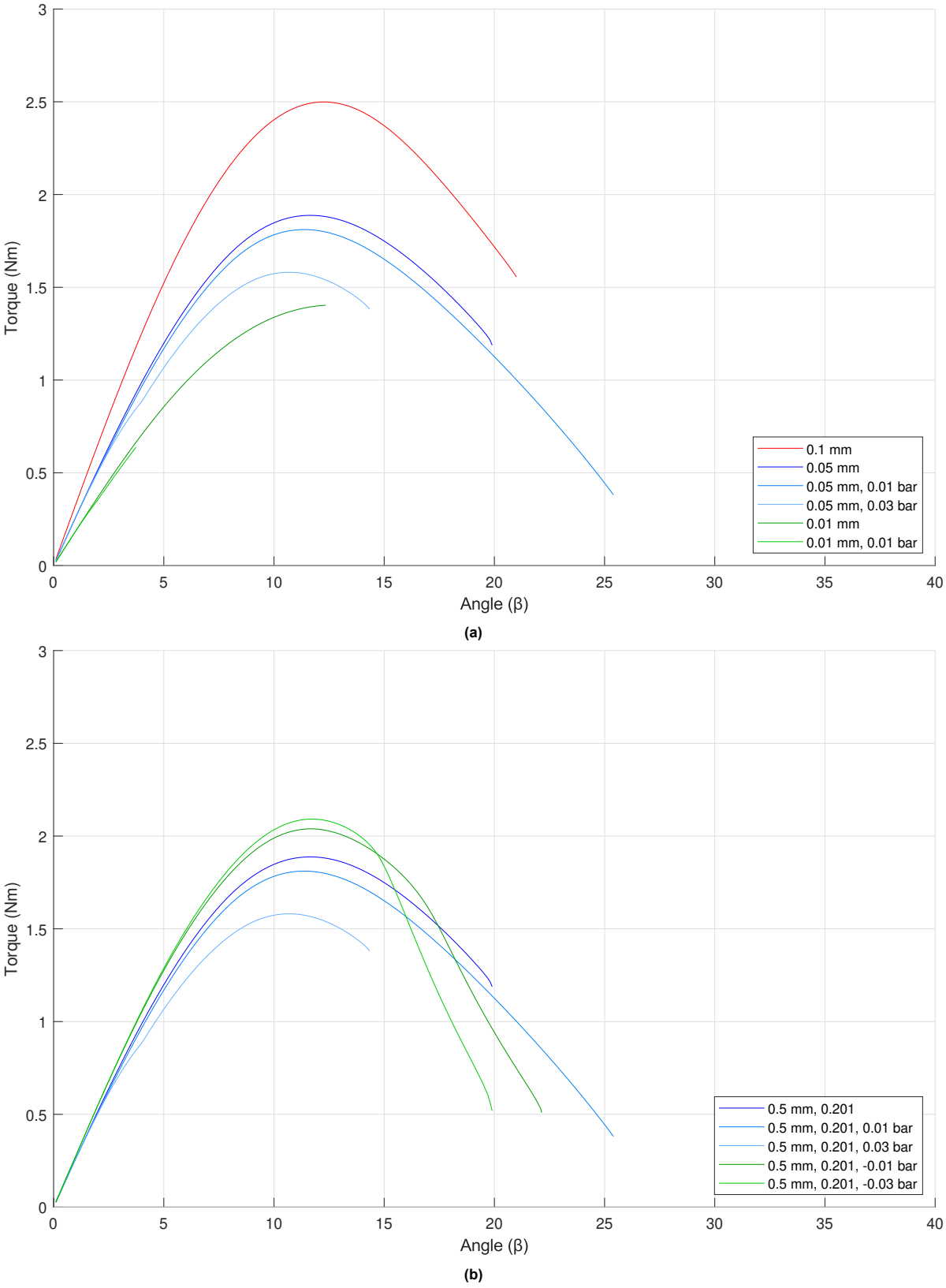

Figure 3.10: (a) Simulation results with parameters t: 0.5 mm and f: 0.201 modeled with decreasing crease thickness indicated by the first legend entry and pre-stressed at different levels and (b) with a constant crease thickness of 0.05 mm and increments of positive and negative pre-stress.

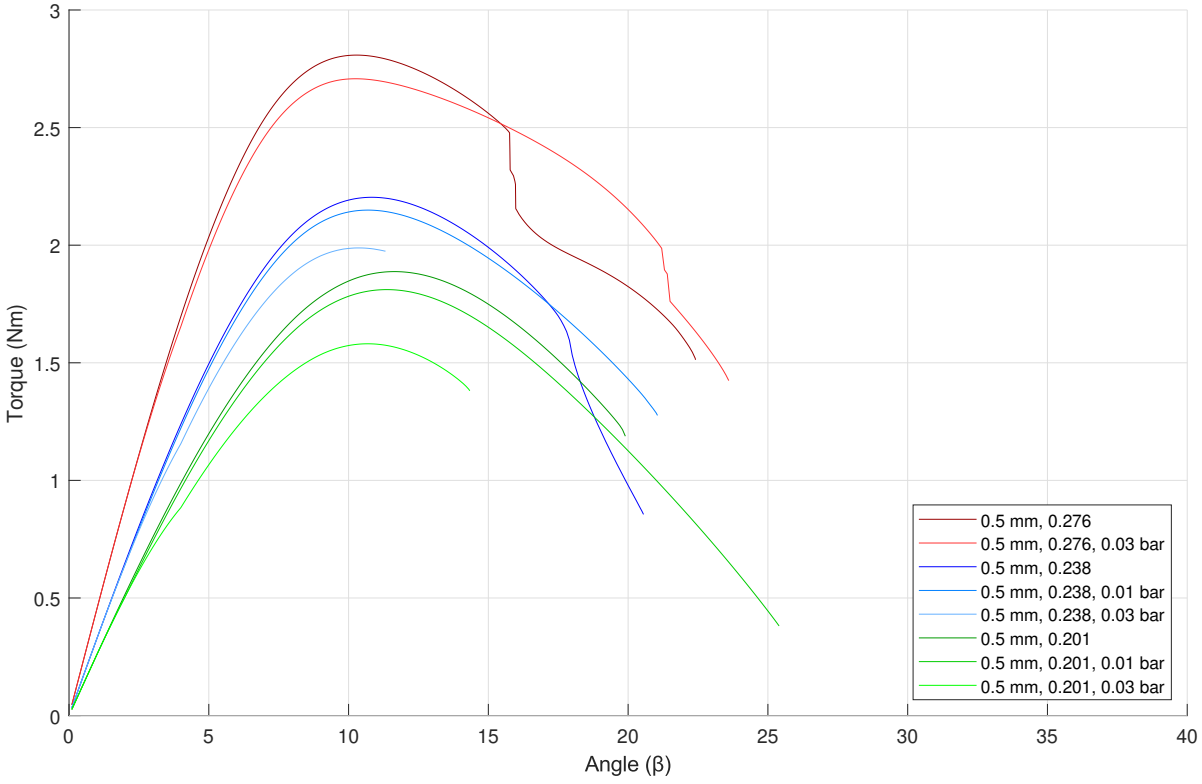

(a)

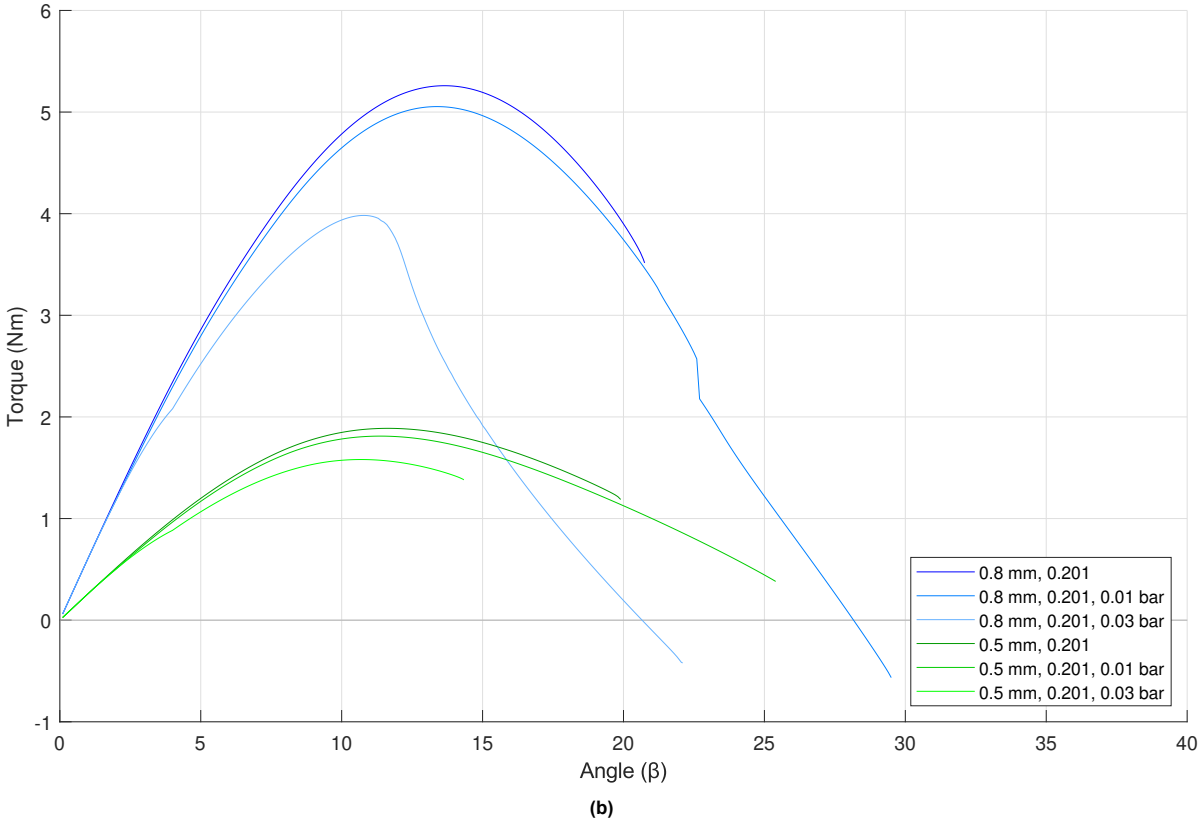

(b)

Figure 3.11: (a) Simulation results with parameters t: 0.5 mm and f: 0.276, 0.238 and 0.201 at different pre-stress levels and (b) simulation results with parameters t: 0.5 mm and 0.8 mm and f: 0.201 at different pre-stress levels.

4

Discussion

This research started with the problem that for prestressing multiple neutrally stable mechanisms simultaneously, remotely and reversibly, limited methods exist. The results for the prototypes tested show that it is possible to prestress neutrally stable mechanisms using negative pressure on an enclosed volume. The torque-angle behavior of some prototypes changes as expected from the curve visualized in Figure 2.2 to a curve with a neutrally stable midsection. This can best be seen in Figure 3.2. Prestressing beyond the desired curve with neutral stability results in a curve where the outer most minimum/maximum is joined by a straight line, which results in a behavior with 3 instead of 5 equilibrium points. These experiments show that it is possible to provide a remote and reversible prestress on a neutrally stable mechanism. The geometry found in this research might be a start in exploring other neutrally stable, enclosed volume joints. Finding methodologies to design these might be a step towards designing activatable neutrally stable joints and metamaterials. These could be useful in situations where switchable joint- or material characteristics are required. The exact method of pressure application can be varied as well. Future research in this area is not limited by the method of pressure application proposed here, but could explore positive pressure, partially pressured mechanisms or fabrication under pressure.

In general, for most prototypes, a reduction in actuation torque is observed with increasing prestress level. The prototypes where this effect can be best seen have the most air-tight setup. These are joint variations Var2, Var3, Var5 and Var6. Versions Var1 and Var4 do not show a reduction as significant, but they still show a small reduction in actuation torque. These were most likely the two least airtight prototypes, so their prestressed behavior much more closely resembles the behavior of an unstressed joint. This is because the negative pressure on the joint is only present for a limited time during the experiment, as ambient air pressure quickly restores. The change in torque-angle characteristic expected in Figure 2.2 can clearly be seen in Var2, Var3 and Var5, with even the exaggerated curve past neutral stability being visible. Notable is that the range of motion wherein neutral stability can be observed is quite large, namely around 30°. As expected, a higher plate thickness t results in a higher actuation torque. An increase in internal volume fraction f results in higher actuation torque as well, but also a slight downward shift of the curve. To obtain a neutrally stable joint around the zero-line, there is most likely an optimum for the angle of indentation, which both the version with f = 0.238 and f = 0.276 have gone past.

4.1. Experiments

The first notable error source is the play in the torque sensor itself. The shaft connecting the torque sensor and bottom clamp has to have some play in it to prevent damage to the torque sensor. This is observed through play perpendicular to the axes of rotation and play in the rotation itself. The deviation in rotation is observed to occur when the moment changes direction, so it can be assumed that this occurs at the same moments when testing a single prototype. The alignment of the center of the

prototype in relation to the t-beam and torque sensor is expected to have negligible influence, as the t-beam provides an evenly distributed torque on the top plate.

Differences in build quality can be observed when comparing three of the same prototype in Figure 3.7. We can see that this difference mostly manifests itself in terms of a difference in magnitudes. The torque-angle characteristic is practically the same when accounting for misaligned start positions. Asymmetry in terms of small differences in plate dimensions, crease width, plates misalignment and small plastic deformations can result in earlier buckling of different sides of the joint, which can cause a rotation of the top plate in the plane that is not constrained. Small jumps can be seen in some results which occur due to the edges of vertical plates ”flipping over”, as seen in Figure 3.6. This happens due to the vertical plates changing their direction of bending after a change of moment direction. Another important point is that of the duct tape attachment to the PP plates. Due to testing the prototypes under water for leakages, some water inevitably manages to get inside the enclosed space, affecting the attachment of the duct tape. Through observation this only seemed to cause detachment of the vertical plates, which are mostly loaded in compression, so is estimated to have negligible effect for the overall behavior of the cube.

4.2. Fabrication recommendations

An important limitation of this research is the measurement range of the torque sensor. A sensor with a larger range could enable larger and/or stiffer prototypes, which could be of interest in future research. This could also enable the testing of stiffer materials and smaller indentation angles. A step towards practical applications compared to the test setup would be to move towards a truly enclosed volume joint. If the joint itself is sealed air-/watertight, there is no need for an external layer around the joint which seals it. To automate the manufacturing process of an enclosed volume joint, it is recommended to look at resin based 3D-printing methods like stereolithography (SLA). These enable more freedom with hollow structures and could require less support structures at overhangs than deposition-based 3D-printing methods. There would still need to be drainage holes to remove excess resin and possibly support structures, which means the joint still has to be made air-/watertight after printing. It is at this stage also important to think about placing an access point to the hollow middle of the joint, like a valve, if it is desired to change the volume inside the joint. The resolution of the printer will determine how thin the creases of the joint can be made compared to the relatively thick plates, which could be a limitation for current printers, due to durability and adhesion of the cured resin. To circumvent this problem, PolyJet printers could be an option. Instead of relying on a single material to achieve all the desired properties, the creases could be printed from a different, more flexible material, and would subsequently not have to be as thin to have the same stiffness. These are however more limited in material choice compared to SLA-printers, only being able to print low-viscosity materials which can creep and lose shape at 45-50 °C.

A more general recommendation would be to manufacture the joint without the top and bottom part, so without needing large overhangs or small access points to reach the hollow part, with any desired and suitable method. The top and bottom parts are then manufactured separately and fastened to the rest of the joint. It then has to be made air-/watertight and any desired access point has to be placed. This method could be more preferable to the above mentioned 3D-printing methods, depending on the ability to securely fasten both parts. Considerations have to be made in terms of desired materials, ease of sealing the joint, time and cost to determine the best method for a given application.

4.3. Finite Element Analysis

The FEA has some notable differences compared to the experiments. Firstly, the creases in the simulation are modeled as thin parts of the same material (PP), while in the experiments they consist of duct tape, which has different material properties. The most notable difference is the much lower Young’s modulus of approximately 10 MPa compared to 1.46 GPa. Also, the thickness of the creases in the FEA is higher than the thickness of the duct tape (0.05 mm compared to about 0.01 mm), due to lower thicknesses having notably more convergence issues. This can be seen in Figure 3.10a, where mod-

els with a crease thickness of 0.01 mm stop significantly earlier due to errors. This means that the behavior of the joint will be more rigid in the simulations, which results in higher torque and possibly a different curve towards neutral stability. Secondly, the FEA models pressure as linearly increasing and then constant, whereas in experiments, pressure depends on the fixed prestressed volume and joint deformation. This was deliberately done for simplicity. A more accurate representation would relate pressure to the internal volume, which would require defining a deforming volume object inside the joint or calculating the internal volume from the deformed geometry each step. With this information, an equation for the internal pressure depending on the internal volume could be implemented. An alternative way could be to approximate this by estimating the volume geometrically at different points in the range of motion and defining a spring or spring and damper, for which the equations depend purely on the angle. In general, the observation that reduced actuation force is needed as the level of prestress is increased, is consistent in both the FEA as well as the experiments. The FEA fails however in capturing the neutrally stable behavior. Improving the current model could be done by simplifying the geometry, optimizing the mesh and letting a more robust model run back and forth with increasing prestress. A more elegant way would be to implement the geometry as a thin-walled structure and neglect the 3-dimensionality of the different thicknesses of plates and creases and only define their properties.

5

Conclusion

Prior to this research, prestressing neutrally stable mechanisms had limits with regards to targeting multiple flexures at once, remotely, reversibly and in a relatively small timeframe. This limited the design flexibility for including a multitude of them in mechanisms or metamaterials and left little possibility for remote prestressing. This research manages to provide a start towards alleviating these limits by prestressing a neutrally stable joint using a negative internal pressure. Some of the prototype joints follow the expected shift in torque-angle curve closely and manage to reach a state of neutral stability for an approximate range of motion of 30°. While the methods explored here are still not sufficient in providing adequate solutions for the first two limits, namely simultaneous and remote prestressing, they can still be seen as a stepping stone towards better solutions in this regard. A pressure stimulus can be universally applied and often does not need great accessibility. Arguably, prestressing using a thermal stimulus is able to tackle these two problems, but it lacks in specificity and timeliness. The experimental setup used in this research does show fast and reversible prestressing, which offers a lot of possibilities for future applications. Further steps in realizing remote and activatable prestress for multiple neutrally stable mechanisms could be the development of a design methodology for neutrally stable closed volume joints and in parallel the development of easier methods for pressure application. Exploring this area with regards to tuneable stiffness or direct fabrication and simultaneous activation of neutrally stable joints could also be interesting.

References

[1] L. L. Howell, “Introduction to compliant mechanisms,” in *Handbook of Compliant Mechanisms*. John Wiley Sons, Ltd, 2013.

[2] M. Schenk and S. D. Guest, “On zero stiffness,” *Proceedings of the Institution of Mechanical Engineers, Part C: Journal of Mechanical Engineering Science*, 2014.

[3] J. A. Gallego and J. L. Herder, “Criteria for the static balancing of compliant mechanisms,” in *International Design Engineering Technical Conferences and Computers and Information in Engineering Conference*, 2010.

[4] J. Gallego Sánchez, “Statically balanced compliant mechanisms,” *TU Delft Repository*, 2013. DOI: `https://doi.org/10.4233/uuid:081e3d0e-173b-4a36-b8d6-c29c70eb7ae3`.

[5] C. Yang, B. Wang, S. Zhong, C. Zhao, and W. Liang, “On tailoring deployable mechanism of a bistable composite tape-spring structure,” *Composites Communications*, 2022.

[6] E. Kebadze, S. Guest, and S. Pellegrino, “Bistable prestressed shell structures,” *International Journal of Solids and Structures*, 2004.

[7] A. A. Nobaveh, J. L. Herder, and G. Radaelli, “Compliant variable negative to zero to positive stiffness twisting elements,” *Mechanism and Machine Theory*, 2024.

[8] X. Lachenal, S. Daynes, and P. M. Weaver, “A non-linear stiffness composite twisting i-beam,” *Journal of intelligent material systems and structures*, 2014.

[9] G. Chaudhary, S. Ganga Prasath, E. Soucy, and L. Mahadevan, “Totimorphic assemblies from neutrally stable units,” *Proceedings of the National Academy of Sciences*, 2021.

[10] R. Mak, A. Amoozandeh Nobaveh, G. Radaelli, and J. L. Herder, “A curved compliant differential mechanism with neutral stability,” *Journal of Mechanisms and Robotics*, 2024.

[11] R. Chen, X. Li, Z. Yang, J. Xu, and H. Yang, “A variable positive-negative stiffness joint with low frequency vibration isolation performance,” *Measurement*, 2021.

[12] R. Hamzehei, M. Bodaghi, and N. Wu, “Mastering the art of designing mechanical metamaterials with quasi-zero stiffness for passive vibration isolation: A review,” *Smart Materials and Structures*, 2024.

[13] A. Valipour, M. H. Kargozarfard, M. Rakhshi, A. Yaghootian, and H. M. Sedighi, “Metamaterials and their applications: An overview,” *Proceedings of the Institution of Mechanical Engineers, Part L: Journal of Materials: Design and Applications*, 2022.

[14] J. T. Overvelde, T. A. De Jong, Y. Shevchenko, *et al.*, “A three-dimensional actuated origami-inspired transformable metamaterial with multiple degrees of freedom,” *Nature communications*, 2016.

[15] D. D. Sonneveld, J. P. Nijssen, and R. A. van Ostayen, “Compliant joints utilizing the principle of closed form pressure balancing,” *Journal of Mechanical Design*, 2023.

[16] O. Faltus, M. Jirásek, M. Horák, *et al.*, “Towards active stiffness control in pattern-forming pneumatic metamaterials,” *European Journal of Mechanics-A/Solids*, 2025.

A

Experimental results

In the following graphs, the raw data for one run of each prestress level is given for all the prototype variations.

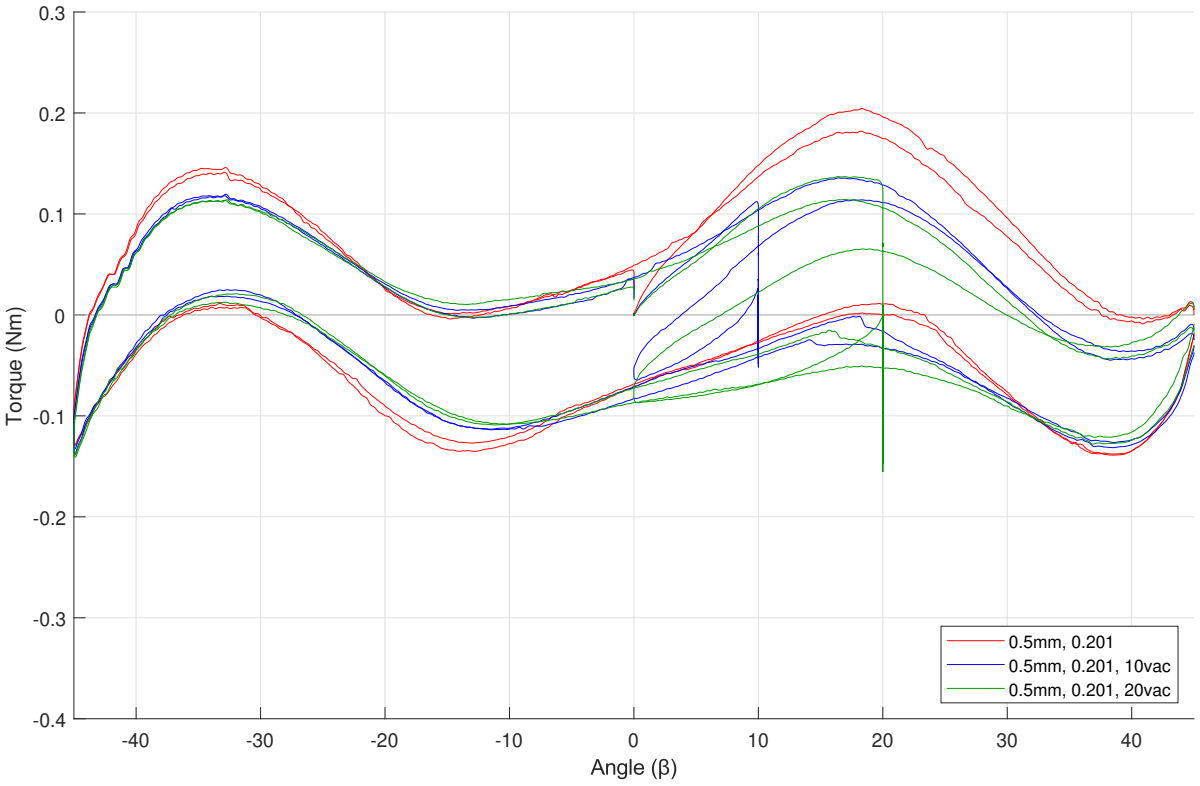

(a)

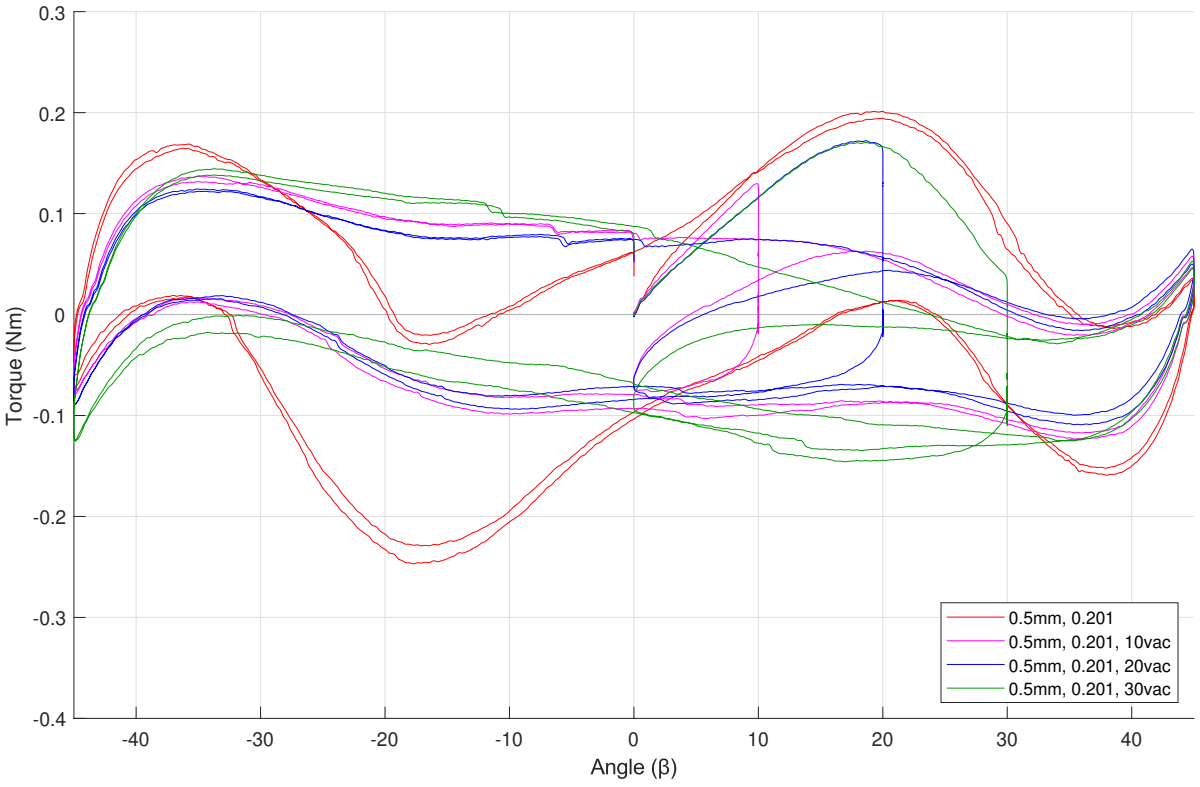

(b)

Figure A.1: (a) Joint Var1 with parameters t: 0.5 mm, f: 0.201 and (b) joint Var2 with parameters t: 0.5 mm, f: 0.201.

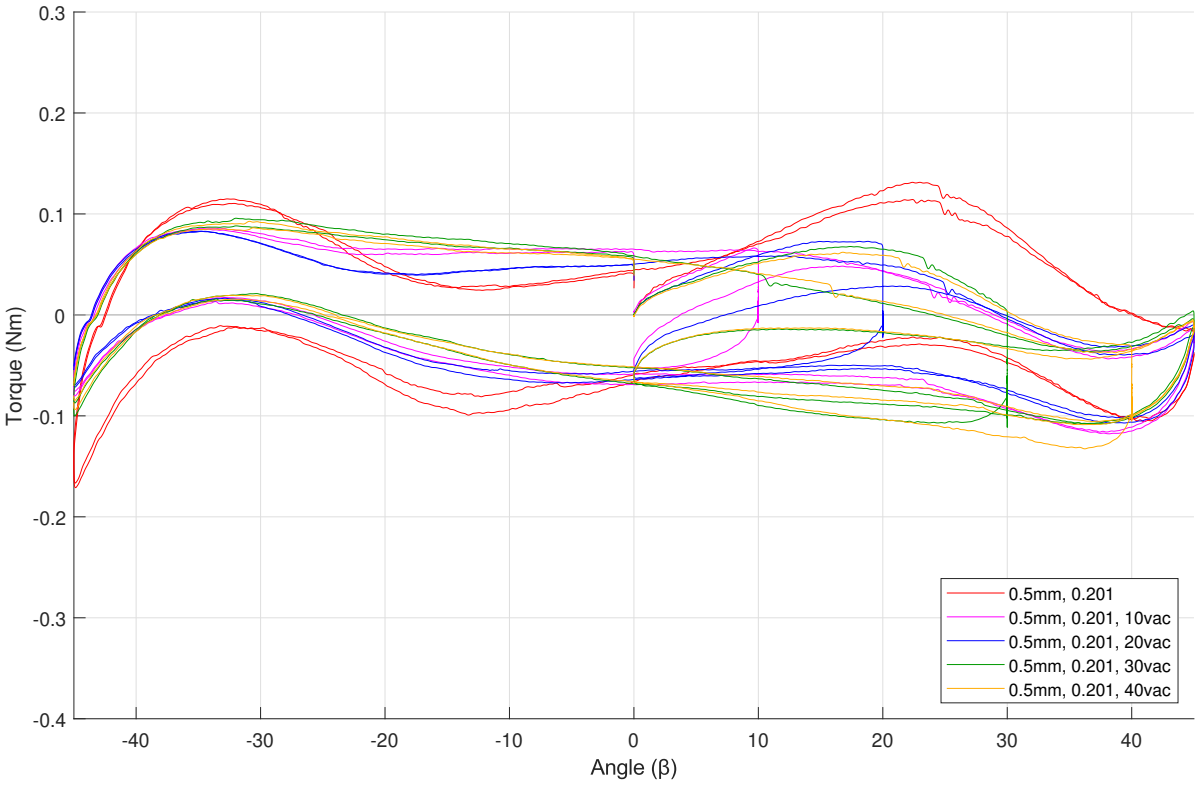

(a)

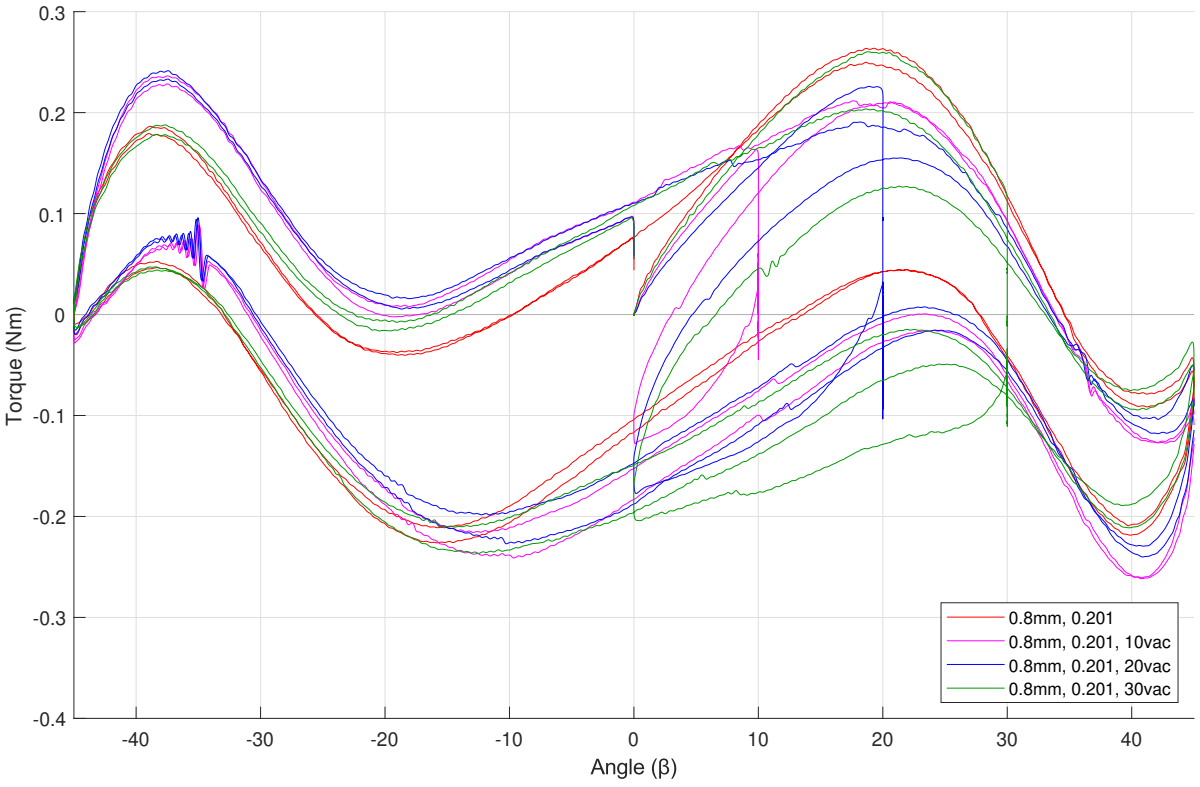

(b)

Figure A.2: (a) Joint Var3 with parameters t: 0.5 mm, f: 0.201 and (b) joint Var4 with parameters t: 0.8 mm, f: 0.201.

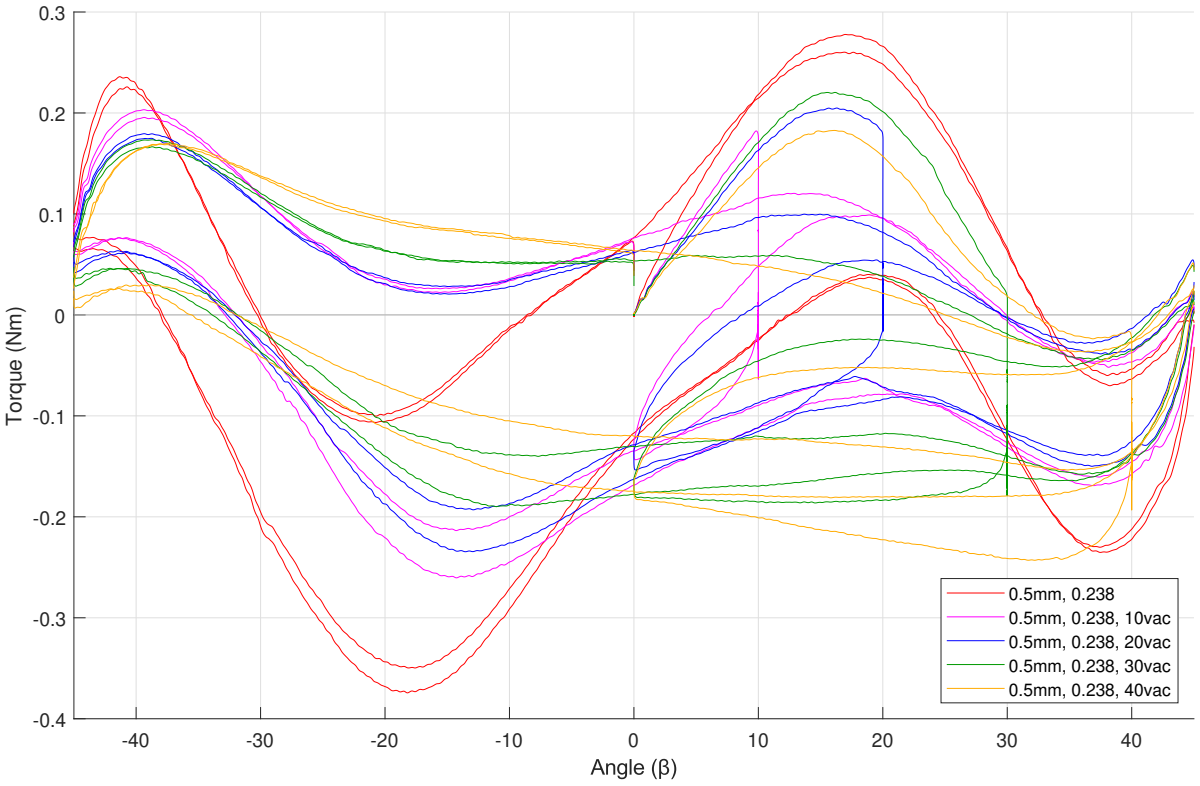

(a)

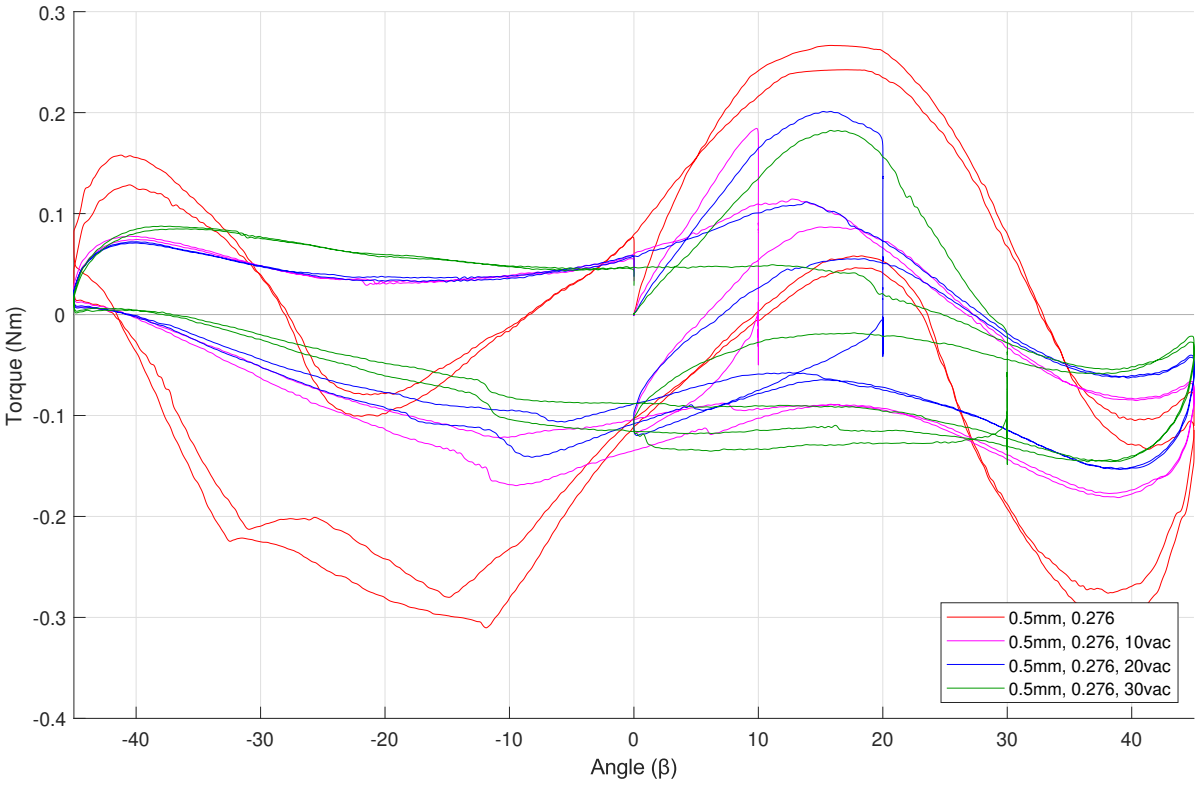

(b)

Figure A.3: (a) Joint Var5 with parameters t: 0.5 mm, f: 0.238 and (b) joint Var6 with parameters t: 0.5 mm, f: 0.276.